INGV-T3 Research Project 2015-2016

HYPSTHER

HYBRID GROUND MOTION PREDICTION EQUATIONS FOR PSHA PURPOSES: THE STUDY CASE OF SOUTHERN ITALY

Task 2 (WG-T2)
Ground Motion Simulation

Maria D'Amico[(1)], Mara Monica Tiberti[(2)],
Emiliano Russo[(3)], Antonio Gomez-Capera[(1)]

Istituto Nazionale di Geofisica e Vulcanologia:
(1) Sezione di Milano, Via Corti 12, 20133 Milano, Italy
(2) Sezione di Roma 1, Via di Vigna Murata 605, 00143 Roma, Italy
(3) Centro Nazionale Terremoti, Via di Vigna Murata 605, 00143 Roma, Italy

Abstract

In this deliverable both strategies and outcomes of the implementation of a synthetic dataset (HYPST_dtb), useful for the generation of hybrid ground motion prediction equations for Southern Calabria and Sicily, will be presented and discussed. Due to the paucity of near source strong motion records in Southern Italy, the Task 2 Working Group of the HYPSTHER project ("Ground motion simulation") has developed different strategies of simulation to made available a huge quantity (more than 180.000 records) of synthetic ground motion data for various intensity measures (PGA, PGV, SA at 0.3, 1, and 3 s). Simulations were performed for hard rock conditions (NERPH A, Vs>2000 m/s). The moment magnitude range is between 3.5 and 7.5 and more than half of the dataset relates to receivers located in the distance range 0-25 km. In order to account for the complex geodynamic framework of the study area, all fault mechanism (normal, reverse and strike slip) are represented into the HYPST_dtb.
The majority of HYPST_dtb record are relatively centered on a set of empirical model ensuring the reliability of the simulations. The variability of the explored synthetic ground motion is heteroscedastic, with smaller values for larger earthquakes. The main contribution to the data variability derives from different combinations of rupture velocities, nucleation points and stress parameters.

Introduction

The Task 2 Working Group of the HYPSTHER project ("Ground motion simulation") is responsible to perform ground motion simulations for the Southern Italy useful to integrate the ground motion database produced by the WG-T1 ("Empirical flat-file generation").

Even if the WG-T1 empirical flat-file represents the most complete and finest collection of both weak and strong motion data for Southern Calabria and Sicily (about 3000 three-component waveforms generated by 174 earthquakes with magnitude between 3.5 and 6.0, and recorded by about 230 accelerometric and/or velocimetric sensors in the time frame 1978-2016), it is not fully representative of the effective seismogenic potential of the considered area.

The Calabria-Sicily region is a very active area that encompasses a wide range of geodynamic settings. The area was struck in the past by several disastrous events reaching a MCS intensity of X-XI (6<M<7.4). For example, the 1783 earthquake sequence, the S. Eufemia Gulf earthquake (September 8, 1905; Mw 7.0), the Messina earthquake (December 28, 1908; Mw 7.1), and the South-eastern Sicily earthquakes (January 11, 1693; Mw 7.4).

In the WG-T1 empirical flat-file, however, records of strong earthquakes (M>6) are lacking and there are few moderate-to-strong earthquakes (M>5) in the observation period. In general, the azimuthal coverage of the recording stations is scarce. Several earthquakes with magnitudes between 4.0 and 5.0 are localized in offshore with epicentral distances respect to the nearest recording stations greater than 50 km.

On that basis, the WG-T2 has been performed region specific deterministic scenarios following three different techniques: the EXSIM (Extended Fault Simulation; Motazedian and Atkinson, 2005; Boore, 2009; Assatourians and Atkinson, 2015), to model a set of Generic Sources (GS) embedded into the crust structure beneath southern Italy, the SMSIM (Stochastic-Method SIMulation; Boore, 2003, 2005) to model point-like sources (PLS) characterized by low magnitudes (3.5<=Mw<5.0), different depth of the simulated events and source-to-site log-spaced distances up to 200 km and the DSM (Deterministic Stochastic Method; Pacor et al., 2005) to model composite seismogenic sources (CSS) around the three sites of interest (Priolo Gargallo, Milazzo and Gioia Tauro).

The first two strategies meet the project requirements, thus making available a huge amount of synthetic ground motion data (more than 180,000 records stored into the HYPST_dtb flat-file) for Hard-Rock Sites (NEHRP A, Vs >= 2000 m/s) and for various intensity measures (PGA, PGV, SA at 0.3, 1, and 3 s). The magnitude range spans between 3.5 and 7.5. About 1/3 of the data are relative to magnitude larger than 7.0 and more than half of the dataset relates to receivers located in the distance range 0-25 km. Finally, the dataset is mainly composed by normal and reverse events, rather than strike-slip ones; PLS simulations are treated as "undefined" fault mechanism.

The third strategy is the basis of further development of the project. The main intent is to provide a synthetic dataset (GAF_SI_dtb) to develop nonparametric ground motion attenuation models useful for region- and site-specific Probabilistic Seismic Hazard Analysis.

At this stage, only the outcomes of the HYPST_dtb will be described and discussed in terms of reliability of data, statistical distribution and parametric variability.

Geodynamic framework

The Calabrian Arc is one of the most seismically active regions of Southern Italy. Its complex geological structure is largely inherited from the early stages of the convergence of the Africa and Eurasia plates. The subduction of oceanic crust that began about 80 Ma along a roughly E-W boundary (Faccenna et al., 2001) continues into present along a rather small (~150 km) portion of the arc between the two continental blocks of Apulia and Hyblei. The evolution of this section of the arc is controlled by a roll-back that started in the Late Miocene (8-10 Ma; Goes et al., 2004; Faccenna et al., 2005), due to the sinking of the Ionian Mesozoic oceanic crust. The effect of plate convergence upon subduction gradually decreased with the progressive rotation and southeastward migration of the Calabrian Arc due to continental collision in Sicily (e.g. Cifelli et al., 2008). Nowadays, tectonic processes in Calabria are controlled mainly by the roll-back process rather than by simple plate convergence.
On the contrary, tectonic processes in Sicily seems to be more directly affected by Africa and Eurasia convergence that, according to current kinematic plate models, acts along a north-northwest to northwest direction at 3 to 8 mm/y (e.g. Nocquet, 2012).
Considerations based on geodetic data indicate 5 mm/y as a tentative subduction rate in the Calabrian Arc (Devoti et al., 2008). Contraction has led to the formation of a large accretionary wedge currently in the Ionian offshore, obtained by progressive folding of the thick sedimentary cover (Cernobori et al., 1996; Merlini et al., 2000; Minelli and Faccenna, 2010; Polonia et al., 2011; Maesano et al., 2017).
The Calabrian Arc experienced fast uplift over the past 125 ky (> 1 mm/y; Bordoni and Valensise, 1998; Ferranti et al., 2006).

Seismicity

The study area (southern Calabria and Sicily) is one of the most active regions of the Italian territory and its seismicity encompasses a wide range of geodynamic settings and depths.
As shown in Table 1 and Figures 1, 2, and 3, during the last four centuries it was struck by several crustal earthquakes with Mw≥6.0 and epicentral intensity Io≥8 (MCS) (CPTI15, Rovida et al., 2016). The largest events in Calabria include the main earthquakes belonging to the seismic sequence of February-March 1783, which struck a large region between the southern end of the Gioia Tauro plain and the region south of Catanzaro (Mw 7.03); the 16 November 1894 earthquake near the northern end of the Messina Straits (Mw 6.12); the 8 September 1905 earthquake in the Gulf of Sant' Eufemia (Mw 6.95); and the 28 December 1908 earthquake in the Messina Straits (Mw 7.10), that ranks among the most catastrophic events in Italian history (Io=11; Fig. 2). Other Mw>6.0 earthquakes affected central Calabria on 4 April 1626 (Mw 6.07), 5 November 1659 (Mw 6.57) and 13 October 1791 (Mw 6.14).
As regards Sicily, the largest earthquake that hit the island was the 11 January 1693, Eastern Sicily event (M_w 7.32). This earthquake was preceded by a large foreshock on 9 January (M_w 6.07). Additional significant earthquakes are the 10 March 1786 (Mw 6.14) and 15 April 1978 (Mw 6.03) events, both of which hit the northern coast of the island between Patti, Milazzo and the Eolian Islands, while the northern offshore hosted two earthquakes of magnitude greater

than 5.0, the 5 March 1823 (Mw = 5.81) and the 6 September 2002 (Mw = 5.92) events, respectively.
The present-day crustal seismic activity of the study area is mainly distributed in the Tyrrhenian offshore of Sicily, in the Patty Gulf area, along the inner Calabria, and (in some measure) in correspondence of the Nebrodi Mounts (Chiarabba et al., 2015).

During the last decades, several earthquakes of moderate magnitude occurred in the study area even though the shallow seismicity recorded in the upper crust of the Ionian offshore is very limited. In some cases, the moment magnitude is larger than 5.0: 1978 Ferruzzano (M_w 5.2), the 11 May 1947 earthquake (M_w 5.7), located on the Ionian coast of Calabria, and the 26 May 2001 (M_w 4.5; Pondrelli et al., 2006) in the Ionian offshore. As for Sicily, it was affected by the 1978 Patti Gulf (M_w 6.1), the 1979 Sicily Channel (M_w 5.3), the 1980 Eolian Islands (M_w = 5.7) and the 2002 Palermo (M_w 5.9) earthquakes.

Figure 4 represents the focal mechanism distribution of the earthquakes occurred with magnitude greater than 4.0 in Southern Calabria and Sicily during the period 1976-2006 (CMT catalog, Pondrelli et al., 2006).

Along the Calabrian Arc, the focal mechanisms available are not enough to fully describe the seismogenic process acting in the region. Very few events with normal mechanism occurred (i.e. 1978 Ferruzzano earthquake, M_w 5.2). Some normal mechanisms are detectable in correspondence of the Nebrodi Mounts. However, they play a minor role in the complex seismotectonics context of the Southern Italy.

Present-day deep seismicity (Figure 5) provides evidence for a well-developed Benioff plane down to a depth of more than 400 km (Chiarabba et al., 2005; 2015), in agreement with tomography data (Wortel and Spakman, 2000; Piromallo and Morelli, 2003; Piana Agostinetti et al., 2009; Neri et al., 2009).
The hypocenters are mainly located between 200 and 400 km of depth defining a steep subduction angle (~70°) along the NW-SE direction.

Year	Mo	Da	Epicentral Area	Lat [°]	Lon [°]	Io MCS	Mw
1169	2	4	Sicilia sud-orientale	37.215	14.949	10	6.5
1184	5	24	Valle del Crati	39.395	16.193	9	6.75
1542	12	10	Sicilia sud-orientale	37.215	14.944	10	6.68
1626	4	4	Calabria centrale	38.851	16.456	9	6.07
1638	3	27	Calabria centrale	39.048	16.289	11	7.09
1638	6	8	Crotonese	39.279	16.812	10	6.76
1659	11	5	Calabria centrale	38.694	16.249	10	6.57
1693	1	9	Sicilia sud-orientale	37.141	15.035	8-9	6.07
1693	1	11	Sicilia sud-orientale	37.140	15.013	11	7.32
1743	2	20	Ionio settentrionale	39.847	18.774	9	6.68
1783	2	5	Calabria meridionale	38.297	15.970	11	7.1
1783	2	7	Calabria centrale	38.580	16.201	10-11	6.74
1783	3	28	Calabria centrale	38.785	16.464	11	7.03
1786	3	10	Golfo di Patti	38.102	15.021	9	6.14
1791	10	13	Calabria centrale	38.636	16.268	9	6.14
1818	2	20	Catanese	37.603	15.140	9-10	6.28
1832	3	8	Crotonese	39.079	16.919	10	6.65
1836	4	25	Calabria settentrionale	39.567	16.737	9	6.18
1854	2	12	Cosentino	39.256	16.295	10	6.34
1870	10	4	Cosentino	39.220	16.331	9-10	6.24
1894	11	16	Calabria meridionale	38.288	15.870	9	6.12
1905	9	8	Calabria centrale	38.811	16.000	10-11	6.95
1908	12	28	Stretto di Messina	38.146	15.687	11	7.1
1968	1	15	Valle del Belice	37.756	12.981	10	6.41
1978	4	15	Golfo di Patti	38.385	15.086	8	6.03

Table 1 Historical earthquakes occurred in Southern Calabria and Sicily whit magnitude greater than 6.0 (Figures 2 and 3) extracted from CPTI15 (Rovida et al., 2016); all data refer to the parameter default section of the catalog.

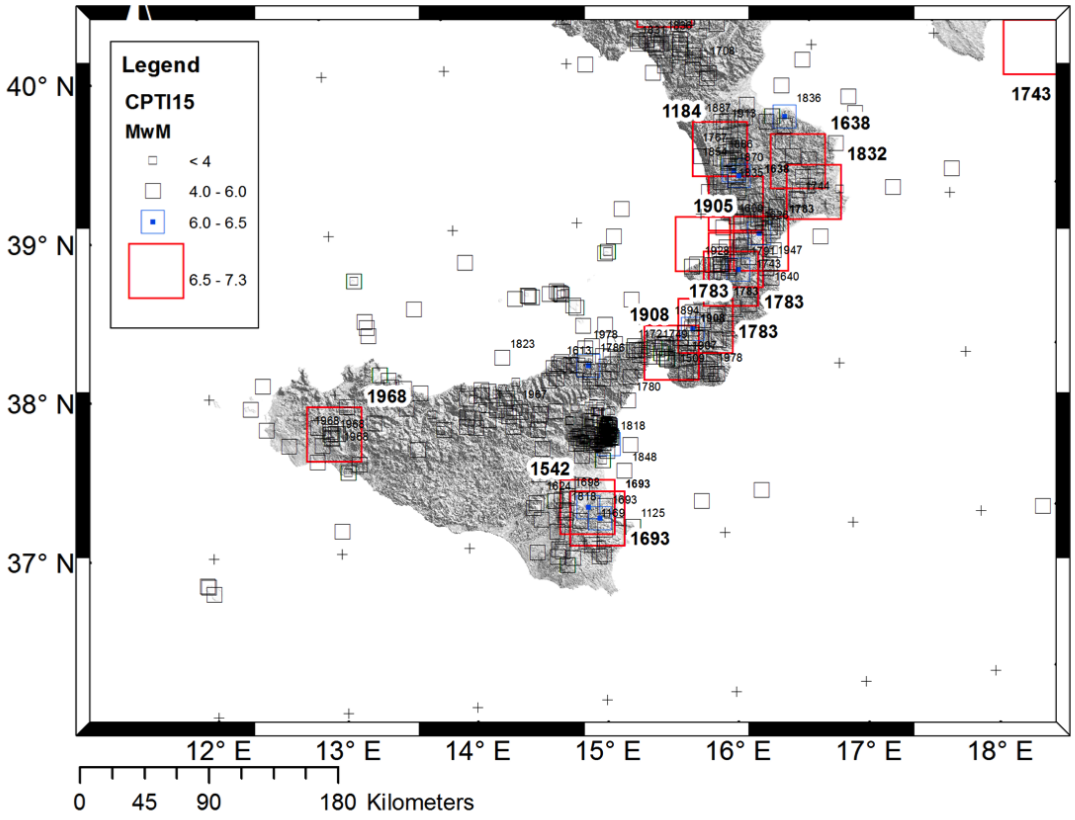

Figure 1 Map of the historical events occurred in Southern Calabria and Sicily (CPTI15, Rovida et al., 2016).

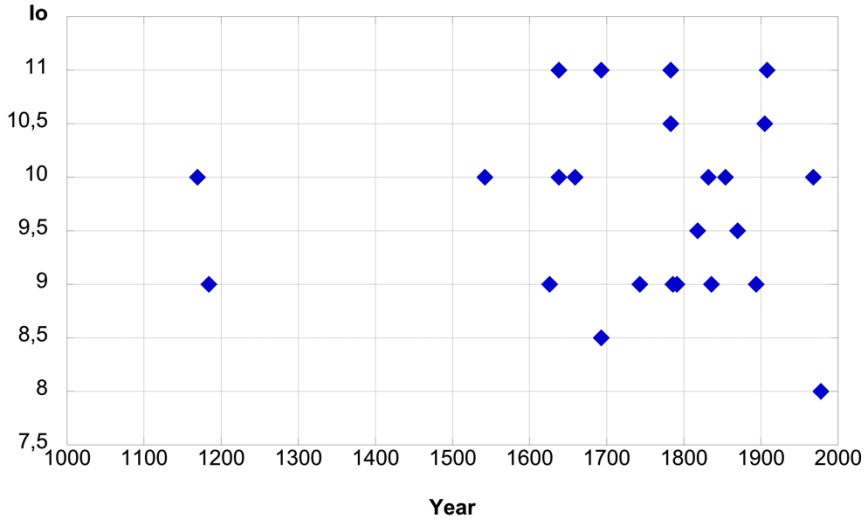

Figure 2 Seismic history (Io) in Southern Calabria and Sicily (CPTI15, Rovida et al., 2016)

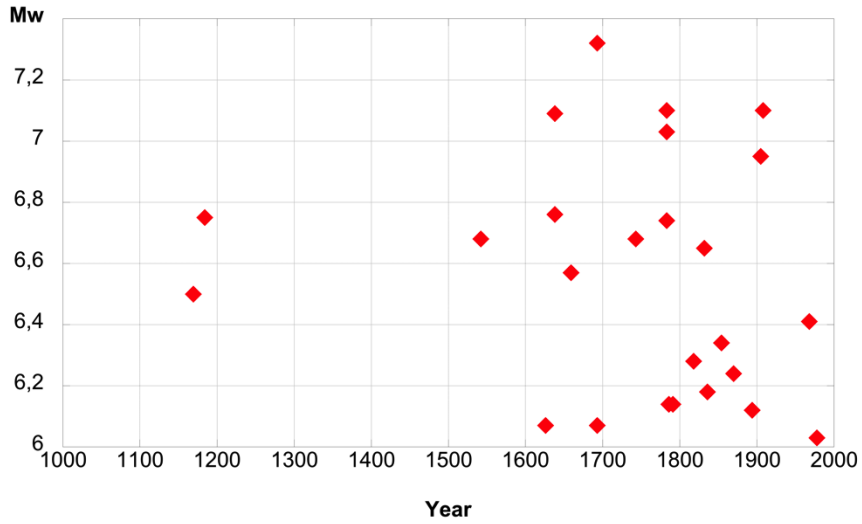

Figure 3 Seismic history (Mw) in Southern Calabria and Sicily (CPTI15, Rovida et al., 2016)

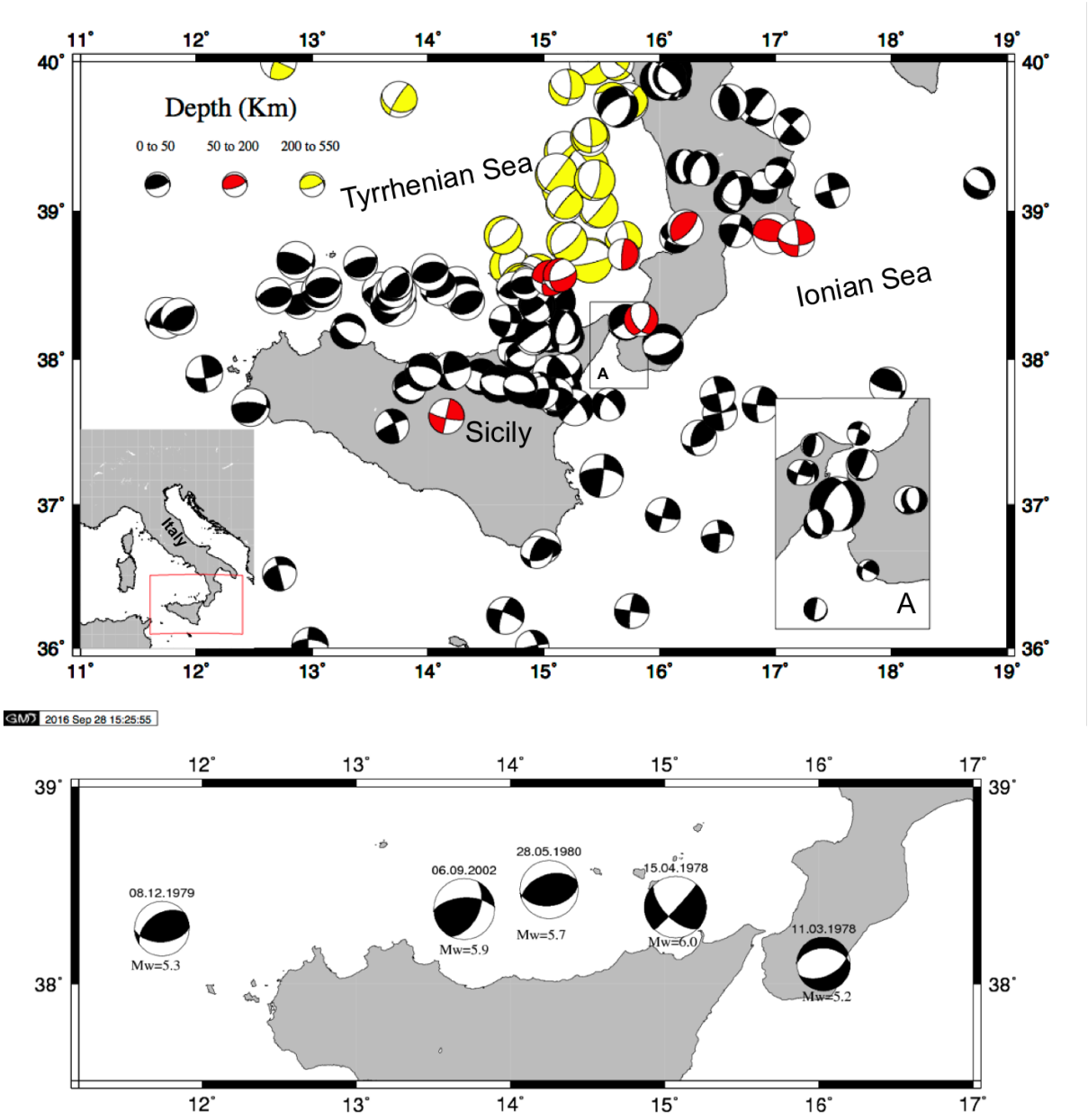

Figure 4 Top: focal mechanisms of the seismic events with M>=4.0 occurred in Southern Calabria and Sicily from the 1976 to the 2006 (CMT, Pondrelli et al., 2006). A: focal mechanisms of the Messina Straits not reported in the CMT catalog and inferred by literature (Gasparini et al., 1985; Bottari et al., 1989; Neri and Wyss, 1993; Neri et al., 1996; Frepoli and Amato 2000); Bottom: CMT focal mechanisms of the major earthquakes (Mw >= 5.0) recorded after the 1978.

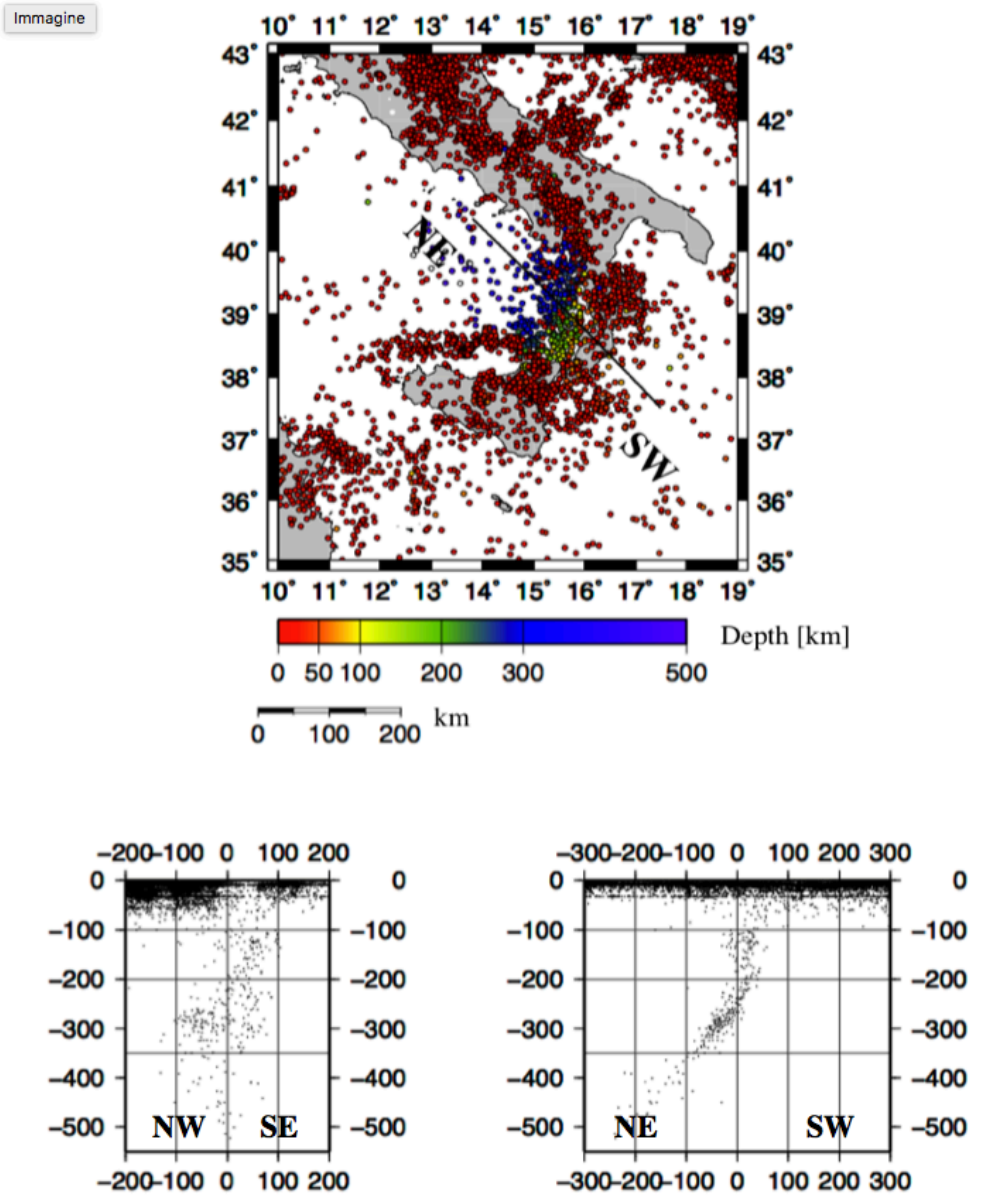

Figure 5 Map of the seismic events occurred in Southern Italy from the 1976 to 2006 (NEIC). In the lowermost part, the seismic events along the Benioff plane of the Tyrrhenian Sea are also reported.

Seismogenic faults

The faulting model used in the HYPSTHER Project is the DISS model (DISS 3.2.0, http://diss.rm.ingv.it/diss/). It is also fully described in Tiberti et al. (2016; Figure 6; Table 2).

The Calabian Arc faulting model consists of a series of blind, low-angle normal faults alternated with strike-slip structures that dissect the Arc, dividing it into portions characterized by a diverse range of geomorphological features and by different uplift rates.

The extensional seismogenic sources are the large east-dipping normal faults underlying the Messina Straits, Gioia Tauro Plain-Mesima River Valley and Sant'Eufemia Basins, from south to north. They are large low-angle normal faults located at a depth between 0 and 13 km along the Tyrrhenian coast, held responsible for the largest earthquakes of Calabria (and of whole Italy): 1908, 1905 earthquakes and part of the 1783 earthquake sequence.

The ITCS016 Aspromonte-Peloritani Composite Source is the southernmost segment of the inner Calabrian extensional fault system, and straddles the marine area between the termination of the Italian peninsula in Calabria and the northeastern tip of Sicily, including the western flank of the Aspromonte Massif (above the city of Reggio Calabria) and the east-facing slope of the Peloritani Mts. (above the city of Messina). It hosts the causative source of the Mw 7.1, 28 December 1908 earthquake. The ITCS082 Gioia Tauro Composite Source straddles the southwestern Tyrrhenian shoulder of southern Calabria, just northeast of the Messina Straits. This source shares a similar low-angle, E-dipping geometry with the nearby ITCS016. It hosts a 25 km long, ESE-dipping low-angle normal fault associated with the Mw 6.6, 5 February 1783 earthquake. North of the Gioia Tauro Plain, the ITCS053 Serre Composite Source straddles the western flank of the Serre Mts. and the Capo Vaticano promontory. This region has been struck by the Mw 6.6, 7 February 1783 Calabria earthquake, the third mainshock of the 1783 sequence. Moving more to the north, the ITCS110 Sant'Eufemia Composite Source straddles the Sant'Eufemia basin (offshore) and the Sant'Eufemia Plain (onland), roughly extending between Vibo Valentia (to the south) and Lamezia Terme (to the north). This is a low-angle, southeast-dipping, fault located in the southwestern portion of the extensional axis of the southern Apennines. It hosts a 25 km long, east-southeast-dipping low-angle normal fault associated with the 8 September 1905 earthquake.

Two major shear zones bound the system to the southwest and to the northeast, respectively. The ITCS068 Composite Seismogenic Source lies at the northern end of the investigated region. It is a near-vertical left-lateral strike-slip fault that stretches E-W between the Sila massif to north and the Serre Mts. to the south. Two additional Composite Seismogenic Sources lying between the ITCS042 and ITCS068 are responsible for the along-strike segmentation of the Calabrian Arc. The ITCS080 Composite Seismogenic Source is the onshore portion of the northernmost of these two lineaments, marking a sharp transition from the uplands of the Serre Mts. to the Gioia Tauro basin, and is thought to act as a transverse feature bounding the Gioia Tauro fault to the north. The ITCS055 Composite Seismogenic

Source is modeled as a high-angle transtensional fault representing the onshore portion of the southernmost lineament. The ITCS042 Composite Seismogenic Source is a near-vertical, right-lateral strike-slip fault that is part of the Tindari-Letojanni Line, an important NNW-trending dextral - or oblique - strike-slip system. A segment of the ITCS042 source has been associated with the Mw 6.1, 15 April 1978 earthquake. It separates extension along the Calabria western coast from contraction in the Southern Tyrrhenian.

In the Ionian offshore, several thrust faults are known to be part of the Calabrian accretionary wedge. They all dip landwards (northwestward) and lie within the inner (pre-Messinian) accretionary wedge. The Western lobe of the accretionary wedge is assumed to host two seismogenic sources in its more internal portions. The innermost of them, the ITCS097, is marked by a major topographic scarp producing a 600-700 m offset in the seafloor (Polonia et al., 2011). These are thrust faults whose seismogenic depth stretches between 4 and 12 km depth. No large earthquake is known for these sources; nevertheless, the size and the geometry of accretionary wedge thrust faults are fully consistent with an expected maximum magnitude of ≥ 7.0 for all corresponding seismogenic sources.

To the West, Sicily is characterized by thrust faults both in the northern offshore (Southern Tyrrhenian) and in the southern part and by prevailing strike-slip tectonics in the Hyblean foreland. In the Southern Tyrrhenian, the ITCS014 and ITCS222 represent the thrust faulting belonging to an E-W narrow contraction belt that runs from the Sicily Channel to the Eolian Islands, about 50 km off the northern Sicily coast. This belt is thought to accommodate part of the Africa-Europe convergence. In the past 30 years several events with Mw>5 originated in this area, including the Mw 5.9 Palermo earthquake of 2002.
Also, SE Sicily hosts large thrust sources, such as the ITCS029 Gela-Catania and ITCS036 Monte Lauro. The reverse/thrust kinematics of the sources bordering to the north and to the south the Catania Plain is in agreement with geological observations and present-day stress field and GPS data, which show NNW-directed active shortening between the Hyblean Plateau and Mt. Etna. This is the area that was struck by the 1693 earthquake sequence. Strike-slip tectonics is also present in the Hyblean foreland, represented by the ITCS035 Ragusa-Palagonia and the ITCS017 Scicli-Giarratana sources. These sources belong to an high-angle, N-S-oriented, 70+ km-long shear zone that extends from the Hyblean foreland area to the inflected foreland buried below the Gela-Catania foredeep deposits and the frontal part of the Apennines-Maghrebide orogenic wedge. This is a long-lasting structure displaying a strong morphological and structural overprint from an older tectonic phase indicating right-lateral displacement along the shear zone. Conversely, geological evidence for the present activity is faint and is given primarily by displaced river courses and marine terraces, all indicating present-day left-lateral sense of motion along the shear zone.

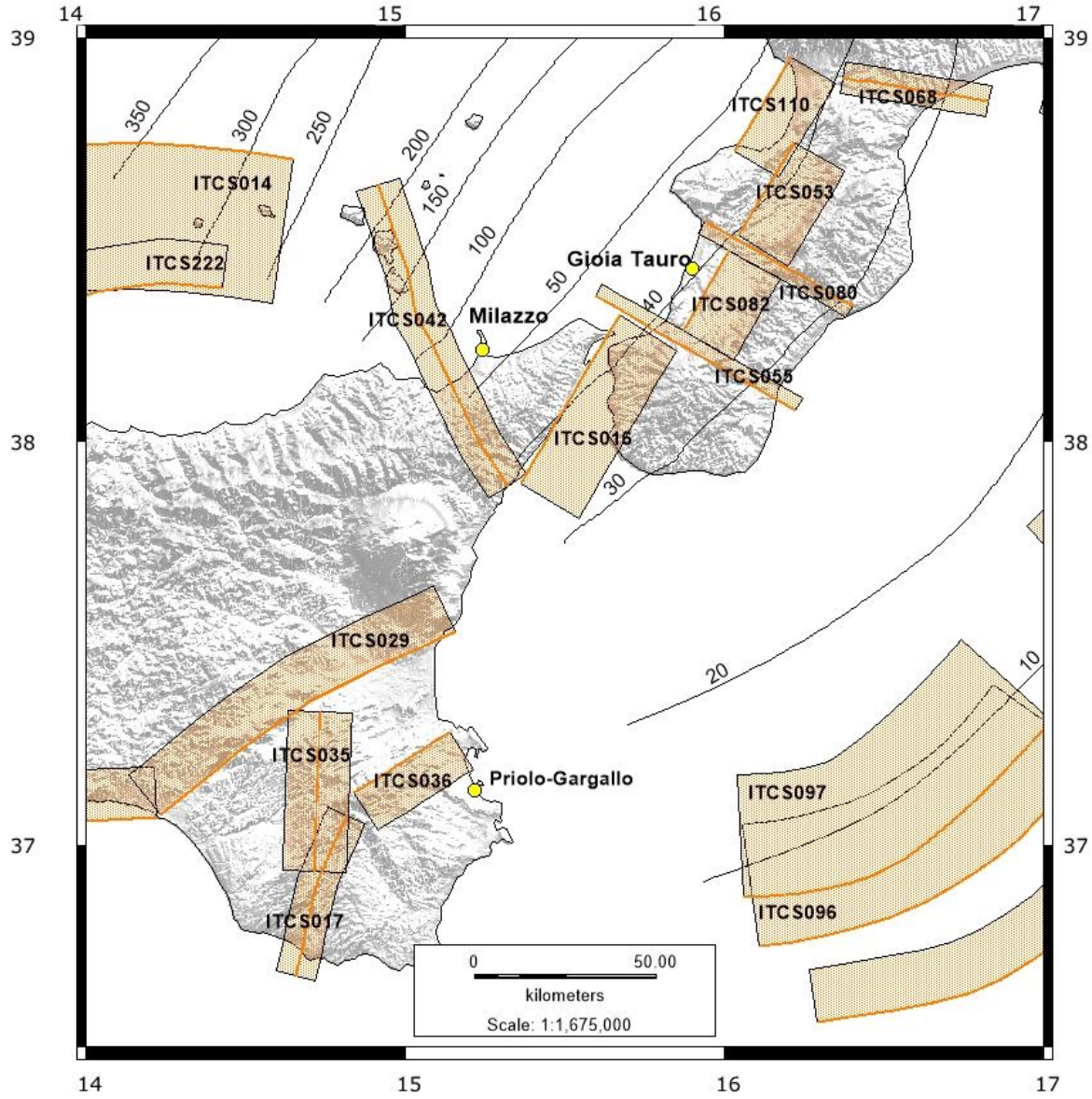

Figure 6 Location of the seismogenic sources mentioned in the text. Thin black lines are the subduction slab isobaths. Yellow dots are the target sites of the project.

ID	Name	Depth	Strike	Dip	Rake	Max M
ITCS110	Sant'Eufemia	0.5-12	25-35	35-45	260-280	6.8
ITCS053	Serre	3.0-11	20-40	20-40	260-280	6.6
ITCS082	Gioia Tauro	3.0-11	20-40	20-40	260-280	6.6
ITCS016	Aspromonte-Peloritani	2.0-13	20-40	25-40	250-280	7.0
ITCS097	Calabria offshore S	4.0-12	180-280	10-20	80-100	7.1
ITCS096	Calabria offshore SE	4.0-12	190-270	10-20	80-100	7.1
ITCS068	Caraffa-Squillace Gulf	3.0-20	90-110	70-90	330-10	6.9
ITCS080	Nicotera-Roccella Ionica	3.0-12	110-130	60-80	300-330	6.0
ITCS055	Bagnara-Bovalino	3.0-12	290-310	60-80	210-240	6.0
ITCS042	Patti-Eolie	1.0-25	140-170	70-90	180-220	6.1
ITCS014	Southern Tyrrhenian	2.0-18	40-100	15-40	60-120	6.5
ITCS222	Southern Tyrrhenian S	2.0-18	40-100	15-40	60-120	6.5
ITCS029	Gela-Catania	3.0-10	225-260	20-40	80-100	6.0
ITCS036	Monte Lauro	3.0-15	50-70	40-50	60-90	6.6
ITCS035	Ragusa-Palagonia	1.0-23	355-15	60-90	350-30	5.6
ITCS017	Scicli-Giarratana	1.0-23	10-30	70-90	350-10	5.5

Table 2 List of the seismogenic sources mentioned in the text and their main parameters.

Ground motion simulations

The Task 2 Working Group of the HYPSTHER project ("Ground motion simulation") is responsible to perform ground motion simulations for the Southern Calabria and Sicily, useful to integrate the ground motion database produced by the WG-T1 ("Empirical flat-file generation").
The WG-T1 empirical flat-file relates to seismic events and stations localized in Southern Calabria and Sicily and include, to date, about 3000 three-component waveforms generated by 174 earthquakes with magnitude between 3.5 and 6.0, and recorded by about 230 accelerometric and/or velocimetric sensors in the time frame 1978-2016. The WG-T1 dataset represents the most complete and finest collection of both weak and strong motion data for Southern Calabria and Sicily, although it is not fully representative of the seismogenic potential of the understudy area. We notice a lack of information either due to the insular/peninsular geomorphology of the area and to the low occurrence rate of moderate-to-strong earthquakes (M>5) in the observation period. In general, the azimuthal coverage of the recording stations is scarce. Several earthquakes with magnitudes between 4.0 and 5.0 are localized in offshore with epicentral distances respect to the nearest recording stations greater than 50 km. Most of all, intensity measures of strong earthquakes (M>6) are lacking. To fill the gaps in the empirical flat-file, we assembled a complementary dataset (HPST_db) by using synthetic ground motion data. To this end, we performed a number of region-specific shaking scenarios at the bedrock (for PGA, PGV and PSA for 0.1, 1, and 3 s) varying: i) magnitude of the simulated events; ii) location and kinematic parameters of individual ruptures; iii) stress parameter; iv) dip of the simulated fault; v) style of faulting.

Simulation methods

We simulated the ground motion by means of three different methods as follows:

1. ***Extended fault SIMulation*** (EXSIM, Motazedian and Atkinson, 2005; Boore, 2009; Assatourians and Atkinson, 2015) to model a set of Generic Sources (GS) embedded into the crust structure beneath southern Italy. GS are not defined by geophysical or geological data. They were constructed for several moment magnitudes (from 5.0 to 7.0 with a step of 0.5), top fault depths, fault mechanisms, and dip angles by means of a procedure that will be illustrated in a further section of the report. In this case we did not use equally spaced simulation grids. The geometry of the simulation sites varies in function of moment magnitude and dip, so that the location of the phantom receivers is denser over and in proximity of the Earth's surface projection of the fault.

2. ***Stochastic-Method SIMulation*** (SMSIM; Boore, 2003, 2005) to model point-like sources (PLS) characterized by lower magnitudes (3.5<=M<5.0), different depth of the simulated events and source-to-site log-spaced distances up to 200 km.

3. ***Deterministic Stochastic Method*** (DSM, Pacor et al., 2005) to model composite seismogenic sources (CSS) around the three sites of interest (Priolo Gargallo, Milazzo and Gioia Tauro). The so-called "composite faults" coming from the DISS 3.2.0 database (http://diss.rm.ingv.it/diss/; Basili et al., 2008) and are seismogenic faults that are exploited well beyond the simple identification of active faults or youthful tectonic features. CS are characterized by geometric (strike, dip, width, depth) and kinematic (rake) parameters based on surface and subsurface geological and geophysical data.

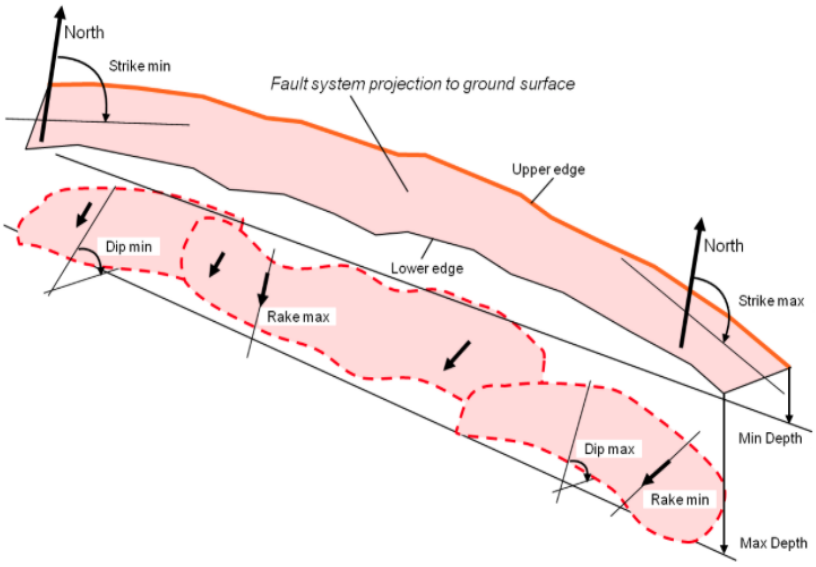

Figure 7 - Parameters of a Composite Seismogenic Source (CSS)

The size of the expected earthquake ruptures, however, is poorly defined or unknown; hence a typical CSS spans an unspecified number of Individual Sources. As a result, such types of sources are not assumed to be capable of a specific-size earthquake. This category of sources was conceived to achieve completeness of the record of potential earthquake sources, although this may imply a smaller accuracy in their description. For such reasons, we modeled different seismogenic ruptures lying over the CSS adopting three earthquake moment magnitudes: M5.0, M6.0, and M7.0. In this way, the composite source represents the Parent Fault (PF) of our set of simulation, while each modeled rupture is handled as a Child Faults (CF) as in D'Amico et al. (2017). For each magnitude, we obtained the equivalent seismic moment using the classical relationships by Kanamori et al. (1975) and Hanks and Kanamori (1979) for constant static stress drop of 30 bars. It seems to be reliable for the study area in the magnitude range 5-7 (Caporali et al., 2011). We then derive fault area and slip from seismic moment, assuming a rigidity of 30 GPa. Length and width (rounded values) are then determined by assuming an aspect ratio of ~1.5.
Simulations were performed over grids of regularly spaced phantom receivers centered on the three test sites. At this stage of the project only the area around Priolo-Gargallo was considered, being the proposed procedure transferable to the other two sites (Milazzo and Gioia Tauro).

Propagation Medium Properties

The regional parameters related to the propagation medium properties are fixed for all simulations. We used a 1D multilayered model (Table 3) representative of the study area in agreement with seismic imaging studies for southern Italy (Barberi et al., 2004; Orecchio et al., 2011; D'Amico et al., 2011). In Table 4 we report the attenuation models produced for the Calabria, the Messina Straits and the Southeastern Sicily (Godano et al., 1992; Giampicciolo et al., 2002; Scognamiglio et al., 2005; Tuvè et al., 2006; Giampicciolo et al., 2006; D'Amico, 2010). The differences in the attenuation model are ascribable to the different geostructural settings of the Calabria-Sicily region. To simulate the ground motion, we considered both the quality factor and the geometrical spreading obtained for the Calabria and for the Northeastern Sicily by D'Amico (2010) to account a broad validity range in terms of source-to-site distances.

Table 3
Crustal velocity model

Depth [km]	Vp [km/s]	Vs [km/s]	ρ [g/cm3]
0	4.50	2.49	2.50
5	5.00	2.76	2.50
8	6.00	3.31	2.60
15	6.50	3.59	2.70
18	6.80	3.76	2.80

30	7.50	4.14	2.90
40	7.50	4.76	2.90

Data from (Barberi et al., 2004; Orecchio et al., 2011; D'Amico et al., 2011). Vs=Vp/1.81 (km/s).

Table 4

Attenuation models for Calabria-Sicily region

Model	area	Q(f)	Geometrical spreading		Distance range [km]
DMC10*	Calabria and Messina Straits	$190f^{0.65}$	$r^{-1.0}$ $r^{-0.5}$	1<r<100 km r>=100 km	10-250
TVE06	Messina Straits	$76f^{0.50}$	_		
GDN92	Messina Straits	$79f^{0.80}$	_		
SML05	Southeastern Sicily	$400f^{0.26}$	r^{-1} $(1/40)(40/r)^{-0.4}$	r<=40 km r>40 km	1-70
GMP02	Southeastern Sicily	$79f^{0.90}$	_		
GMP06	Southeastern Sicily	$49f^{0.88}$	_		

Data from (D'Amico 2010: DMC10; Tuvè et al., 2006: TVE06; Godano et al., 1992: GDN92; Scognamiglio et al., 2005: SML05; Giampicciolo et al., 2002: GMP02; Giampicciolo et al., 2006: GMPC06). An asterisk marks the attenuation model used to simulate the ground motion.

Source Parameters of Generic Sources

The simulated events are normal (NF), reverse (RF) and strike-slip (SS) earthquakes at six magnitudes (5.0, 5.5, 6.0, 6.5, 7.0 and 7.5). Dip and top depth of the simulated faults vary in function of magnitude as described in Table 5, while the strike is fixed along the North direction. Point-like source are modeled for lower magnitudes (3.5, 4.0, and 4.5). On the whole, we generated 62 different extended fault geometries and 12 point-like sources.

Table 5

Sources geometries and mechanisms for Generic Source Simulations

M_w	Top Depth [km]	Style of Faulting	Dip [°]	# EXTENDED/POINTS SOURCES
7.5; 7.0	1; 5	N	30; 60	20

		R	30; 60	
		S	90	
	5; 10; 15	N	45	
6.5; 6.0		R	45	18
		S	90	
	5; 10; 15; 20	N	45	
5.5; 5.0		R	45	24
		S	90	
4.5; 4.0; 3.5	5; 10; 15; 25	--	--	12
				TOT: 74

Table 6 contains additional information on the simulated fault ruptures. For each magnitude, Length and Width of the simulated fault are based on the well-known relations from Wells and Coppersmith (1997), while the sub-faults size (Δl) was specified according to Atkinson and Beresnev's (2002) relationship [1].

$$\log\Delta l = -2 + 0.4M \qquad 4 \leq M \leq 8 \qquad [1]$$

Table 6

Faults Size

Mw	5.0			5.5			6.0			6.5			7.0		
Style of Faulting	N	R	S	N	R	S	N	R	S	N	R	S	N	R	S
Length [km]	4	3	3	7	6	7	13	11	14	23	22	29	42	44	59
Width [km]	4	3	4	6	4	5	9	7	7	14	11	10	20	18	13
Sub-fault Size [km x km]	1 x 1			2 x 2			3 x 3			4 x 4			6 x 6		

Source Parameters of Composite Sources

Firstly, we considered all the CSS defined in the DISS 3.2.0 database of Italian faults (http://diss.rm.ingv.it/diss/; Basili et al., 2008) around the site of Priolo Gargallo. After that, we modeled different seismogenic ruptures floating over the CSS adopting three earthquake moment magnitudes: M5.0, M6.0, and M7.0. In this way, the composite source represents the Parent Fault (PF) of our set of simulation, while each modeled rupture is handled as a Child Faults (CFs). For the computation of the synthetic ground motion for M7.0 and M6.0 we only considered CFs at source-to-site distances less than 200km (red and blue boxes in Figure 8), whereas for M5.0 we modeled a set of ruptures floating over the PF closest to Priolo Gargallo (yellow boxes in Figure 8). Tables 6a, 6b and 6c, report the fault-rupture parameters of Child Faults for magnitude 7.0, 6.0 and 5.0, respectively.

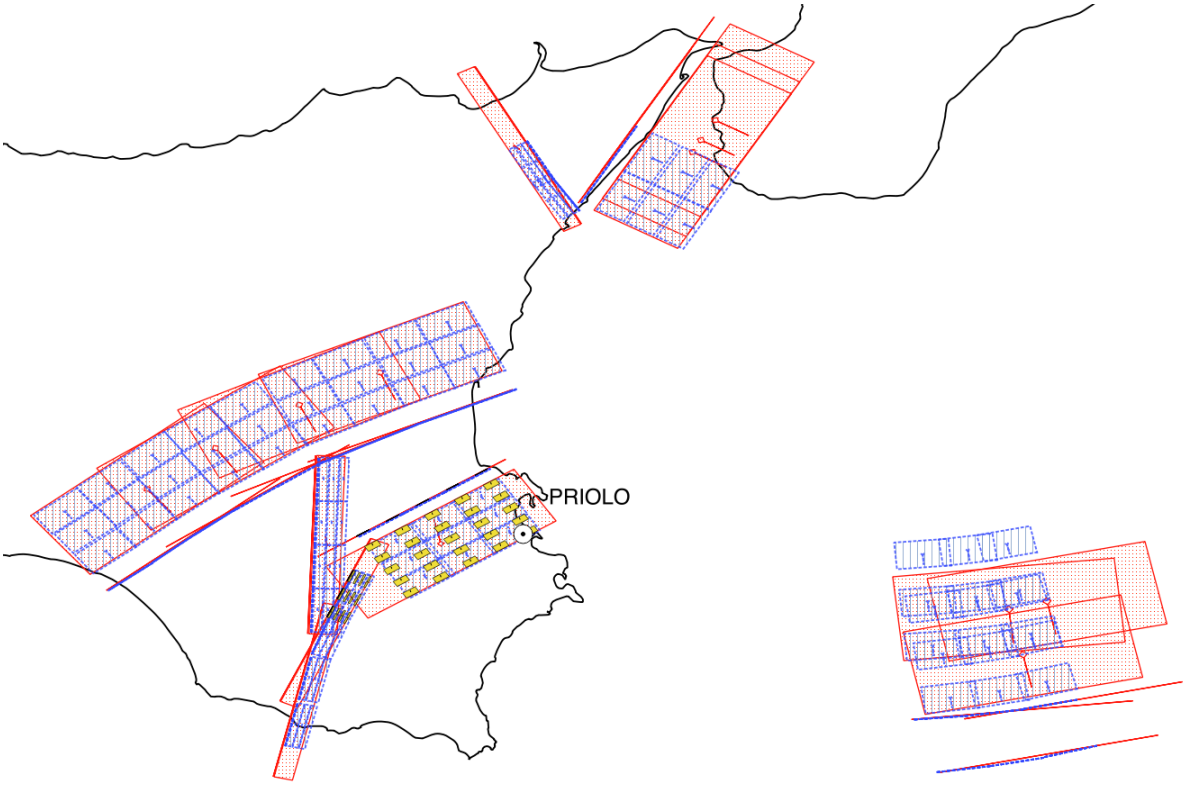

Figure 8 Map of the CFs modeled for the site of Priolo Gargallo

ID	Length [km]	Width [km]	Min Depth [km]	Max Depth [km]	Strike [°]	Dip [°]	Rake [°]	LatSL [°]	LonSL [°]	LatSR [°]	LonSR [°]	LatUL [°]	LonUL [°]	LatUR [°]	LonUR [°]	LatLR [°]	LonLR [°]	LatLL [°]	LonLL [°]
701	45	22	2	12.7	30	29	270	37.934	15.345	38.284	15.602	37.918	15.380	38.268	15.638	38.182	15.829	37.831	15.570
702	45	22	2	12.7	30	29	270	37.907	15.326	38.257	15.583	37.891	15.361	38.241	15.619	38.155	15.809	37.804	15.551
703	45	22	2	12.7	30	29	270	37.979	15.377	38.329	15.634	37.963	15.413	38.313	15.670	38.227	15.861	37.876	15.603
708	45	22	1	22.7	152	80	200	38.217	15.092	37.860	15.333	38.216	15.090	37.859	15.331	37.843	15.293	38.200	15.051
716	45	22	3	18.6	57	45	70	37.105	14.735	37.326	15.161	37.083	14.754	37.303	15.180	37.186	15.276	36.965	14.849
717	45	22	3	14	246	30	90	37.484	15.177	37.319	14.712	37.527	15.153	37.362	14.688	37.519	14.600	37.683	15.065
718	45	22	3	14	244	30	90	37.419	14.995	37.242	14.537	37.461	14.969	37.284	14.512	37.438	14.417	37.615	14.874
719	45	22	3	14	235	30	90	37.359	14.807	37.127	14.391	37.397	14.773	37.165	14.357	37.305	14.234	37.538	14.649
720	45	22	3	14	231	30	90	37.283	14.650	37.028	14.255	37.319	14.613	37.065	14.219	37.198	14.083	37.453	14.477
721	45	22	4	9.7	258	15	90	36.700	16.641	36.616	16.148	36.831	16.606	36.747	16.113	36.934	16.063	37.018	16.556
722	45	22	4	9.7	264	15	90	36.778	16.584	36.736	16.082	36.912	16.566	36.869	16.064	37.059	16.039	37.102	16.541
727	45	22	1	22.3	2	75	10	36.930	14.712	37.334	14.730	36.930	14.715	37.334	14.733	37.333	14.797	36.928	14.779
728	45	22	1	22.7	24	80	360	36.777	14.649	37.147	14.855	36.776	14.651	37.146	14.857	37.132	14.896	36.762	14.690
729	45	22	1	22.7	13	80	360	36.606	14.634	37.000	14.748	36.606	14.636	37.000	14.750	36.992	14.791	36.598	14.677
730	45	22	4	9.7	258	15	90	36.821	16.696	36.737	16.202	36.952	16.661	36.868	16.167	37.055	16.117	37.139	16.611

Table 6a Fault-rupture parameters of Child Faults for magnitude 7.0; average displacement 1.3 m.

ID	Length [km]	Width [km]	Min Depth [km]	Max Depth [km]	Strike [°]	Dip [°]	Rake [°]	LatSL [°]	LonSL [°]	LatSR [°]	LonSR [°]	LatUL [°]	LonUL [°]	LatUR [°]	LonUR [°]	LatLR [°]	LonLR [°]	LatLL [°]	LonLL [°]
6001	11	7	3	6.5	246	30	90	37.4848	15.1774	37.4446	15.0635	37.5275	15.1534	37.4873	15.0396	37.5371	15.0116	37.5773	15.1254
6002	11	7	3	6.5	243	30	90	37.4046	14.9517	37.3597	14.8408	37.4462	14.925	37.4013	14.8141	37.4499	14.7829	37.4948	14.8938
6003	11	7	3	6.5	235	30	90	37.3209	14.7401	37.2642	14.6382	37.3592	14.7064	37.3024	14.6045	37.3471	14.5652	37.4038	14.667
6004	11	7	3	6.5	232	30	90	37.2129	14.5414	37.152	14.4436	37.2497	14.5053	37.1888	14.4074	37.2318	14.3653	37.2927	14.4631
6005	11	7	3	6.5	232	30	90	37.0905	14.3528	37.0296	14.2551	37.1273	14.3167	37.0664	14.2191	37.1094	14.177	37.1703	14.2746
6006	11	7	10.5	14	232	30	90	37.0884	14.3499	37.0275	14.2522	37.2173	14.2236	37.1564	14.126	37.1993	14.0839	37.2602	14.1814
6007	11	7	10.5	14	232	30	90	37.2162	14.5485	37.1553	14.4507	37.3451	14.4219	37.2842	14.3242	37.3271	14.282	37.388	14.3797
6008	11	7	10.5	14	236	30	90	37.3206	14.7408	37.2653	14.6377	37.4562	14.6257	37.4009	14.5227	37.4461	14.4843	37.5014	14.5873
6009	11	7	10.5	14	243	30	90	37.4043	14.9522	37.3594	14.8412	37.55	14.8586	37.5051	14.7477	37.5537	14.7165	37.5986	14.8274
6010	11	7	10.5	14	246	30	90	37.4835	15.1759	37.4433	15.0621	37.6329	15.092	37.5927	14.9782	37.6425	14.9502	37.6827	15.064
6011	11	7	3	7.9	57	45	70	37.2505	15.0158	37.3044	15.1201	37.2279	15.0343	37.2818	15.1385	37.2444	15.169	37.1905	15.0647
6012	11	7	3	7.9	57	45	70	37.2001	14.9185	37.254	15.0227	37.1775	14.9369	37.2314	15.0411	37.194	15.0716	37.1401	14.9673
6013	11	7	3	7.9	57	45	70	37.1506	14.8226	37.2045	14.9267	37.128	14.841	37.1819	14.9452	37.1445	14.9756	37.0906	14.8714
6014	11	7	13.7	18.6	57	45	70	37.1511	14.8216	37.205	14.9257	37.0478	14.9057	37.1016	15.0099	37.0643	15.0403	37.0104	14.9361
6015	11	7	13.7	18.6	57	45	70	37.2006	14.9164	37.2545	15.0206	37.0973	15.0006	37.1511	15.1048	37.1138	15.1353	37.0599	15.031
6016	11	7	13.7	18.6	57	45	70	37.251	15.0137	37.3049	15.118	37.1477	15.0979	37.2015	15.2023	37.1642	15.2327	37.1103	15.1284
6017	11	7	1	7.9	24	80	0	36.9838	14.7643	37.0742	14.8147	36.9832	14.7661	37.0735	14.8165	37.0691	14.829	36.9787	14.7786
6018	11	7	1	7.9	22	80	0	36.8855	14.7147	36.9772	14.7611	36.8849	14.7165	36.9766	14.7629	36.9725	14.7756	36.8808	14.7292
6019	11	7	1	7.9	13	80	0	36.782	14.6853	36.8784	14.7131	36.7816	14.6873	36.878	14.7151	36.8756	14.7284	36.7792	14.7006
6020	11	7	1	7.9	13	80	0	36.6767	14.6544	36.7731	14.6821	36.6763	14.6563	36.7727	14.6841	36.7703	14.6974	36.6739	14.6696
6021	11	7	16.1	23	13	80	0	36.6767	14.6544	36.7731	14.6822	36.671	14.6854	36.7673	14.7132	36.7649	14.7265	36.6685	14.6987
6022	11	7	16.1	23	13	80	0	36.782	14.6847	36.8784	14.7125	36.7763	14.7158	36.8726	14.7436	36.8702	14.7569	36.7738	14.7291
6023	11	7	16.1	23	21	80	0	36.8855	14.7153	36.9779	14.7597	36.8764	14.7451	36.9687	14.7895	36.9648	14.8023	36.8724	14.7579
6024	11	7	16.1	23	24	80	0	36.9845	14.7638	37.0749	14.8142	36.9741	14.793	37.0645	14.8435	37.06	14.856	36.9697	14.8055
6025	11	7	1	7.8	2	75	10	37.2313	14.7258	37.3302	14.7301	37.2312	14.7288	37.3301	14.7332	37.3295	14.7536	37.2306	14.7493

ID	Length [km]	Width [km]	Min Depth [km]	Max Depth [km]	Strike [°]	Dip [°]	Rake [°]	LatSL [°]	LonSL [°]	LatSR [°]	LonSR [°]	LatUL [°]	LonUL [°]	LatUR [°]	LonUR [°]	LatLR [°]	LonLR [°]	LatLL [°]	LonLL [°]
6026	11	7	1	7.8	2	75	10	37.1323	14.7214	37.2312	14.7257	37.1322	14.7244	37.2311	14.7287	37.2305	14.7492	37.1316	14.7448
6027	11	7	1	7.8	2	75	10	37.0333	14.7172	37.1322	14.7215	37.0332	14.7202	37.1321	14.7245	37.1315	14.745	37.0326	14.7406
6028	11	7	1	7.8	2	75	10	36.9343	14.7128	37.0332	14.7171	36.9342	14.7158	37.0331	14.7201	37.0325	14.7405	36.9336	14.7362
6029	11	7	16.2	23	2	75	10	36.9352	14.7128	37.0341	14.7171	36.9338	14.7616	37.0327	14.766	37.0321	14.7864	36.9333	14.782
6030	11	7	16.2	23	2	75	10	37.0342	14.7167	37.1331	14.721	37.0328	14.7656	37.1317	14.77	37.1311	14.7904	37.0323	14.786
6031	11	7	16.2	23	2	75	10	37.1332	14.7211	37.2321	14.7255	37.1318	14.7701	37.2307	14.7745	37.2301	14.7949	37.1313	14.7905
6032	11	7	16.2	23	2	75	10	37.2322	14.7253	37.3311	14.7297	37.2308	14.7743	37.3297	14.7787	37.3291	14.7992	37.2303	14.7948
6033	11	7	1	7.9	147	80	200	37.9729	15.2535	37.8899	15.3218	37.972	15.2518	37.8891	15.3201	37.8831	15.3085	37.9661	15.2401
6038	11	7	16.1	23	147	80	200	37.9729	15.2535	37.8899	15.3218	37.959	15.2263	37.876	15.2947	37.8701	15.2831	37.953	15.2147
6039	11	7	4	5.8	262	15	90	36.6297	16.2524	36.6159	16.1303	36.7626	16.2291	36.7489	16.107	36.8091	16.0965	36.8229	16.2185
6040	11	7	4	5.8	255	15	90	36.6756	16.4934	36.65	16.3743	36.8053	16.45	36.7797	16.3309	36.8384	16.3113	36.864	16.4304
6041	11	7	4	5.8	258	15	90	36.78	16.4486	36.7594	16.3278	36.9113	16.4138	36.8908	16.293	36.9502	16.2772	36.9708	16.3979
6042	11	7	4	5.8	265	15	90	36.744	16.2022	36.7354	16.0792	36.8777	16.1876	36.8691	16.0646	36.9297	16.058	36.9383	16.181
6043	11	7	10.2	12	255	15	90	36.6756	16.4934	36.65	16.3743	37.0063	16.3827	36.9807	16.2636	37.0394	16.2439	37.065	16.363
6044	11	7	10.2	12	262	15	90	36.6297	16.2524	36.6159	16.1303	36.9687	16.1929	36.9549	16.0708	37.0152	16.0603	37.0289	16.1823
6045	11	7	10.2	12	265	15	90	36.744	16.2022	36.7354	16.0792	37.085	16.1649	37.0764	16.0419	37.137	16.0353	37.1456	16.1582
6046	11	7	10.2	12	258	15	90	36.78	16.4486	36.7594	16.3278	37.1149	16.3595	37.0943	16.2388	37.1538	16.2229	37.1743	16.3437
6047	11	7	2	5.4	30	29	270	37.9087	15.3261	37.9944	15.3889	37.8925	15.3618	37.9781	15.4245	37.9506	15.485	37.8649	15.4222
6048	11	7	9.6	13	30	29	270	37.9087	15.3261	37.9944	15.3888	37.8308	15.497	37.9165	15.5599	37.889	15.6203	37.8033	15.5573
6049	11	7	3	6.5	230	30	90	37.1544	14.4475	37.0908	14.3525	37.1902	14.4098	37.1266	14.3148	37.1684	14.2708	37.232	14.3658
6050	11	7	3	6.5	235	30	90	37.266	14.6396	37.2093	14.5378	37.3043	14.6059	37.2475	14.5042	37.2922	14.4649	37.3489	14.5666
6051	11	7	3	6.5	243	30	90	37.3596	14.8398	37.3147	14.7289	37.4012	14.8131	37.3563	14.7023	37.4049	14.6711	37.4498	14.7819
6052	11	7	3	6.5	246	30	90	37.4442	15.0631	37.404	14.9493	37.4869	15.0392	37.4467	14.9254	37.4965	14.8974	37.5367	15.0112
6053	11	7	10.5	14	246	30	90	37.4421	15.0589	37.4019	14.9451	37.5915	14.975	37.5513	14.8613	37.6011	14.8333	37.6413	14.947
6054	11	7	10.5	14	243	30	90	37.3593	14.8381	37.3144	14.7272	37.505	14.7446	37.4601	14.6338	37.5087	14.6026	37.5536	14.7134

6055	11	7	10.5	14	235	30	90	37.2666	14.6398	37.2099	14.538	37.4006	14.5218	37.3438	14.4201	37.3885	14.3808	37.4452	14.4825
ID	**Length [km]**	**Width [km]**	**Min Depth [km]**	**Max Depth [km]**	**Strike [°]**	**Dip [°]**	**Rake [°]**	**LatSL [°]**	**LonSL [°]**	**LatSR [°]**	**LonSR [°]**	**LatUL [°]**	**LonUL [°]**	**LatUR [°]**	**LonUR [°]**	**LatLR [°]**	**LonLR [°]**	**LatLL [°]**	**LonLL [°]**
6056	11	7	10.5	14	231	30	90	37.155	14.4499	37.0927	14.3535	37.2821	14.3206	37.2199	14.2243	37.2622	14.1812	37.3245	14.2775
6057	11	7	6.8	10.3	232	30	90	37.0905	14.3528	37.0296	14.2551	37.174	14.271	37.1131	14.1734	37.156	14.1313	37.2169	14.2289
6058	11	7	6.8	10.3	230	30	90	37.1571	14.4512	37.0935	14.3562	37.2382	14.3658	37.1747	14.2708	37.2164	14.2268	37.28	14.3217
6059	11	7	6.8	10.3	232	30	90	37.2138	14.5441	37.1529	14.4462	37.2973	14.4621	37.2364	14.3644	37.2793	14.3222	37.3402	14.4199
6060	11	7	6.8	10.3	235	30	90	37.2651	14.6378	37.2084	14.536	37.3519	14.5614	37.2951	14.4597	37.3398	14.4204	37.3965	14.5221
6061	11	7	6.8	10.3	236	30	90	37.3191	14.7395	37.2638	14.6364	37.4069	14.665	37.3516	14.5619	37.3968	14.5236	37.4521	14.6266
6062	11	7	6.8	10.3	243	30	90	37.3587	14.8391	37.3138	14.7282	37.4531	14.7785	37.4082	14.6677	37.4567	14.6365	37.5017	14.7473
6063	11	7	6.8	10.3	244	30	90	37.4028	14.951	37.3594	14.8391	37.498	14.8925	37.4546	14.7806	37.5036	14.7505	37.547	14.8623
6064	11	7	6.8	10.3	246	30	90	37.4433	15.0629	37.4031	14.9491	37.5401	15.0086	37.4998	14.8948	37.5496	14.8668	37.5899	14.9806
6065	11	7	6.8	10.3	246	30	90	37.4838	15.177	37.4436	15.0632	37.5806	15.1227	37.5403	15.0089	37.5901	14.9809	37.6304	15.0947
6066	11	7	8.3	13.2	57	45	70	37.1506	14.8226	37.2045	14.9267	37.088	14.8736	37.1419	14.9777	37.1045	15.0082	37.0507	14.904
6067	11	7	8.3	13.2	57	45	70	37.2001	14.9185	37.254	15.0227	37.1375	14.9695	37.1914	15.0738	37.154	15.1042	37.1002	14.9999
6068	11	7	8.3	13.2	57	45	70	37.2505	15.0158	37.3044	15.1201	37.1879	15.0669	37.2418	15.1712	37.2044	15.2016	37.1506	15.0973
6069	11	7	8.6	15.4	2	75	10	37.2313	14.7258	37.3302	14.7301	37.2306	14.7518	37.3294	14.7562	37.3289	14.7767	37.23	14.7723
6070	11	7	8.6	15.4	2	75	10	37.1323	14.7214	37.2312	14.7257	37.1316	14.7474	37.2304	14.7517	37.2299	14.7722	37.131	14.7678
6071	11	7	8.6	15.4	2	75	10	37.0333	14.7172	37.1322	14.7215	37.0326	14.7431	37.1314	14.7475	37.1309	14.7679	37.032	14.7635
6072	11	7	8.7	15.5	2	75	10	36.9343	14.7128	37.0332	14.7171	36.9336	14.739	37.0324	14.7434	37.0319	14.7638	36.933	14.7594
6073	11	7	8.3	15.2	24	80	0	36.9838	14.7643	37.0742	14.8147	36.9784	14.7794	37.0688	14.8298	37.0644	14.8423	36.974	14.7919
6074	11	7	8.8	15.7	21	80	0	36.8855	14.7147	36.9779	14.7591	36.8805	14.731	36.9729	14.7754	36.9689	14.7881	36.8766	14.7437
6075	11	7	8.3	15.2	13	80	0	36.782	14.6853	36.8784	14.7131	36.779	14.7013	36.8754	14.7292	36.873	14.7425	36.7766	14.7146
6076	11	7	8.6	15.5	13	80	0	36.6767	14.6544	36.7731	14.6822	36.6736	14.671	36.77	14.6988	36.7676	14.712	36.6712	14.6842
6077	11	7	5.8	9.2	30	29	270	37.9087	15.3261	37.9944	15.3888	37.8616	15.4294	37.9473	15.4922	37.9198	15.5527	37.8341	15.4897
6078	11	7	7.7	14.6	147	80	200	37.9729	15.2535	37.8899	15.3218	37.9662	15.2405	37.8833	15.3088	37.8773	15.2972	37.9603	15.2289
6079	11	7	7	8.8	262	15	90	36.6297	16.2524	36.6159	16.1303	36.8624	16.2116	36.8486	16.0895	36.9088	16.079	36.9226	16.201

6080	11	7	7	8.8	255	15	90	36.6756	16.4934	36.65	16.3743	36.9025	16.4175	36.8769	16.2984	36.9357	16.2787	36.9613	16.3978
ID	**Length [km]**	**Width [km]**	**Min Depth [km]**	**Max Depth [km]**	**Strike [°]**	**Dip [°]**	**Rake [°]**	**LatSL [°]**	**LonSL [°]**	**LatSR [°]**	**LonSR [°]**	**LatUL [°]**	**LonUL [°]**	**LatUR [°]**	**LonUR [°]**	**LatLR [°]**	**LonLR [°]**	**LatLL [°]**	**LonLL [°]**
6081	11	7	7	8.8	265	15	90	36.744	16.2022	36.7354	16.0792	36.978	16.1766	36.9694	16.0536	37.03	16.047	37.0386	16.17
6082	11	7	7	8.8	258	15	90	36.78	16.4486	36.7594	16.3278	37.0098	16.3875	36.9892	16.2667	37.0487	16.2509	37.0693	16.3717
6083	11	7	4	5.8	259	15	90	36.6486	16.3734	36.6297	16.2524	36.7804	16.3414	36.7615	16.2204	36.8212	16.2059	36.8401	16.327
6084	11	7	7	8.8	259	15	90	36.6486	16.3734	36.6297	16.2524	36.8792	16.3174	36.8603	16.1964	36.92	16.1819	36.9389	16.3029
6085	11	7	10.2	12	259	15	90	36.6486	16.3734	36.6297	16.2524	36.9847	16.2918	36.9658	16.1708	37.0255	16.1563	37.0443	16.2773
6086	11	7	4	5.8	262	15	90	36.7584	16.3285	36.7446	16.2062	36.8913	16.3052	36.8776	16.1829	36.9378	16.1723	36.9516	16.2946
6087	11	7	7	8.8	262	15	90	36.7584	16.3285	36.7446	16.2062	36.9911	16.2876	36.9773	16.1654	37.0375	16.1548	37.0513	16.277
6088	11	7	10.2	12	262	15	90	36.7584	16.3285	36.7446	16.2062	37.0974	16.2689	37.0836	16.1466	37.1439	16.136	37.1576	16.2583
6089	11	7	2	5.4	30	29	270	37.996	15.389	38.0817	15.4518	37.9798	15.4247	38.0654	15.4875	38.0379	15.5481	37.9522	15.4851
6090	11	7	5.8	9.2	30	29	270	37.996	15.389	38.0817	15.4518	37.9489	15.4924	38.0346	15.5553	38.0071	15.6158	37.9214	15.5528
6091	11	7	9.6	13	30	29	270	37.996	15.389	38.0817	15.4518	37.9181	15.5601	38.0038	15.6231	37.9763	15.6836	37.8906	15.6205
6092	11	7	1	7.9	151	80	200	38.0467	15.2035	37.9602	15.2643	38.0459	15.2017	37.9594	15.2626	37.9541	15.2504	38.0406	15.1896
6093	11	7	8	14.9	151	80	200	38.0467	15.2035	37.9602	15.2644	38.0405	15.1894	37.954	15.2503	37.9487	15.2382	38.0352	15.1773
6094	11	7	17	23.9	151	80	200	38.0467	15.2035	37.9602	15.2644	38.0336	15.1736	37.9471	15.2345	37.9418	15.2223	38.0283	15.1614

Table 6b Fault-rupture parameters of Child Faults for magnitude 6.0; average displacement 0.5 m.

ID	Length [km]	Width [km]	Min Depth [km]	Max Depth [km]	Strike [°]	Dip [°]	Rake [°]	LatSL [°]	LonSL [°]	LatSR [°]	LonSR [°]	LatUL [°]	LonUL [°]	LatUR [°]	LonUR [°]	LatLR [°]	LonLR [°]	LatLL [°]	LonLL [°]
5001	3	2.1	3	4.5	58	45	70	37.2892	15.0938	37.3035	15.1226	37.2663	15.1118	37.2806	15.1405	37.2693	15.1494	37.255	15.1207
5002	3	2.1	3	4.5	58	45	70	37.2208	14.9582	37.2351	14.9869	37.1979	14.9762	37.2122	15.0049	37.2009	15.0138	37.1866	14.985
5003	3	2.1	3	4.5	58	45	70	37.1526	14.8226	37.1669	14.8513	37.1297	14.8405	37.144	14.8692	37.1327	14.8781	37.1184	14.8494
5004	3	2.1	17.1	18.6	58	45	70	37.1518	14.8248	37.1661	14.8535	37.0214	14.927	37.0357	14.9557	37.0244	14.9645	37.0101	14.9358
5005	3	2.1	17.1	18.6	58	45	70	37.2913	15.0927	37.3056	15.1215	37.1609	15.195	37.1752	15.2238	37.1639	15.2327	37.1496	15.2039
5006	3	2.1	17.1	18.6	58	45	70	37.2208	14.9582	37.2351	14.9869	37.0904	15.0605	37.1047	15.0892	37.0934	15.0981	37.0791	15.0693
5007	3	2.1	10.1	11.6	58	45	70	37.1518	14.8248	37.1661	14.8535	37.0748	14.8852	37.0891	14.9139	37.0777	14.9228	37.0634	14.894
5008	3	2.1	10.1	11.6	58	45	70	37.2208	14.9582	37.2351	14.9869	37.1438	15.0186	37.1581	15.0474	37.1467	15.0562	37.1324	15.0275
5009	3	2.1	10.1	11.6	58	45	70	37.2892	15.0938	37.3035	15.1226	37.2122	15.1543	37.2265	15.183	37.2151	15.1919	37.2008	15.1632
5010	3	2.1	1	3.1	24	80	0	37.049	14.801	37.0736	14.8147	37.0484	14.8028	37.073	14.8166	37.0717	14.8203	37.047	14.8066
5011	3	2.1	1	3.1	24	80	0	36.968	14.7552	36.9926	14.7689	36.9674	14.757	36.992	14.7708	36.9907	14.7745	36.966	14.7608
5012	3	2.1	20.9	23	24	80	0	36.968	14.7552	36.9926	14.7689	36.9545	14.7931	36.9792	14.8068	36.9778	14.8106	36.9532	14.7968
5013	3	2.1	20.9	23	24	80	0	37.049	14.801	37.0736	14.8148	37.0355	14.8389	37.0602	14.8527	37.0588	14.8564	37.0342	14.8427

Table 6c Fault-rupture parameters of Child Faults for magnitude 5.0; average displacement 0.2 m.

Ruptures Kinematic and Stress Parameter

To generate shaking scenarios for GS and CSS ruptures, we used rupture fronts that radially propagate with three different constant velocities. Rupture velocities are defined in terms of percentage of the share waves velocity (V_s) of the embedding fault medium (70%; 80%; 85%). As the Vs increase with depth (Table 2), the rupture velocities vary in function of fault geometries within the medium properties.
To set the nucleation points and the amount of slip over the fault, two different strategies have been drawn up for GS or CSS. In case of GS, we considered only one nucleation point randomly located over the fault and random distributions of slip. In case of CSS, for fault distances greater than 50 km from Priolo-Gargallo we set only a nucleation point in the middle of the fault plane; for the closest CSS, several nucleation points have been set as follows:

1. The M7.0 CFs are subdivided along strike into three sub-faults for each of which we simulate nine nucleation points at a regular spacing along strike and dip. In such a way, both unilateral and bilateral directivity effects can be properly modeled.
2. Being the M6.0 CFs smaller, we simulate only nine nucleation points uniformly distributed on the fault plane.
3. For the M5.0 CFs we simulate only three nucleation points.

The fault slip is assumed as uniformly distributed over each CF plane. Although this hypothesis may seem very simplistic, we use it because in the adopted simulation method the slip distribution has a second-order effect on the ground motion amplitude (Pacor et al., 2005) with respect to the other kinematic parameters (i.e. nucleation point and rupture velocity).

For GS simulation by EXSIM (5.0<=Mw<=7.5) we used 5 different values of the stress parameters (50, 100, 150, 200, and 250 bars), while for GS simulations by SMSIM the stress drop values are randomly sampled from a normal distribution having a mean of 150 bars and a standard deviation of 30 bars (Figure 9).
For CSS simulations by DSM the issue to setup the stress value is addressed by replacing the epistemic uncertainty on the stress parameter with the aleatory uncertainty given by the variability in the fault dimension, nucleation point, and rupture velocity.

Tables 7a and 7b summarize the scenario events performed for GSs and CSS, respectively.

Table 7a Scenario Events performed for GSs for Southern Calabria and Sicily

M	#Nucleation Points	#Rupture velocities	#Modeled sources	#Stress Parameters	#Scenarios	Simulation Method
7.5	1	3	10	5	150	EXSIM
7.0	1	3	10	5	150	EXSIM
6.5	1	3	9	5	135	EXSIM
6.0	1	3	9	5	135	EXSIM
5.5	1	3	12	5	180	EXSIM
5.0	1	3	12	5	180	EXSIM
4.5	1	--	4	19	76	SMSIM
4.0	1	--	4	19	76	SMSIM
3.5	1	--	4	19	76	SMSIM

Table 7b Scenario Events performed for CSS for Priolo-Gargallo

M	# Nucleation Points	#Rupture velocities	#Modeled sources	#Scenarios	Simulation Method
7.0	41	3	15	123	DSM
6.0	162	3	90	486	DSM
5.0	39	3	13	117	DSM

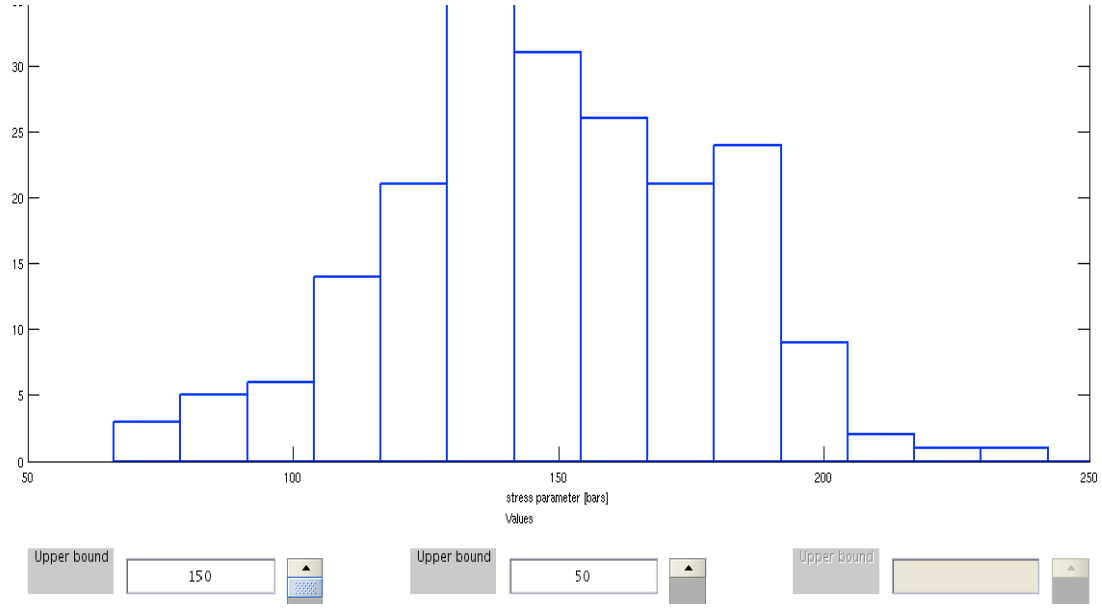

Figure 9 normal distribution used to sample the stress parameter for GSs by using SMSIM (μ = 150 bars; σ = 30 bars)

Site Parameters

Being the final goal of the project the evaluation of the seismic hazard in correspondence of three test sites (Milazzo: E15.278633° N38.202339°; Gioia Tauro: E15.913146° N38.461573°; Priolo Gargallo: E15.192546° N37.177617°), we only simulated scenario events for bedrock conditions. To this end we considered a kappa values of 0.035 s and site amplification factors for hard rock sites (NEHRP A, Vs>=2000 m/s) by Atkinson and Boore (2006). Amplification factors are reported in Table 8.

Table 8
Site Amplification Factors Used in the Simulations for Hard-Rock Sites
NEHRP A (Vs >= 2000 m/s)

Frequency [Hz]	Amplification Factor
0.5	1
1	1.13
2	1.22
5	1.36
10	1.41
50	1.41

Simulation sites

For GS, we simulated the ground motion over grids of phantom receivers constructed around each simulated fault in order to have a denser distribution of stations over and in proximity of the source. The geometry of the GS receivers depends on size and dip of the simulated faults. A common reference point (N: 38.232964°; E: 15.632186°) and strike (0°) were set up for all simulation grids. As an example, Figure 10 represents the simulation grids generated for M7.0, M6.0, and M5.0 for NF and SS fault mechanisms.

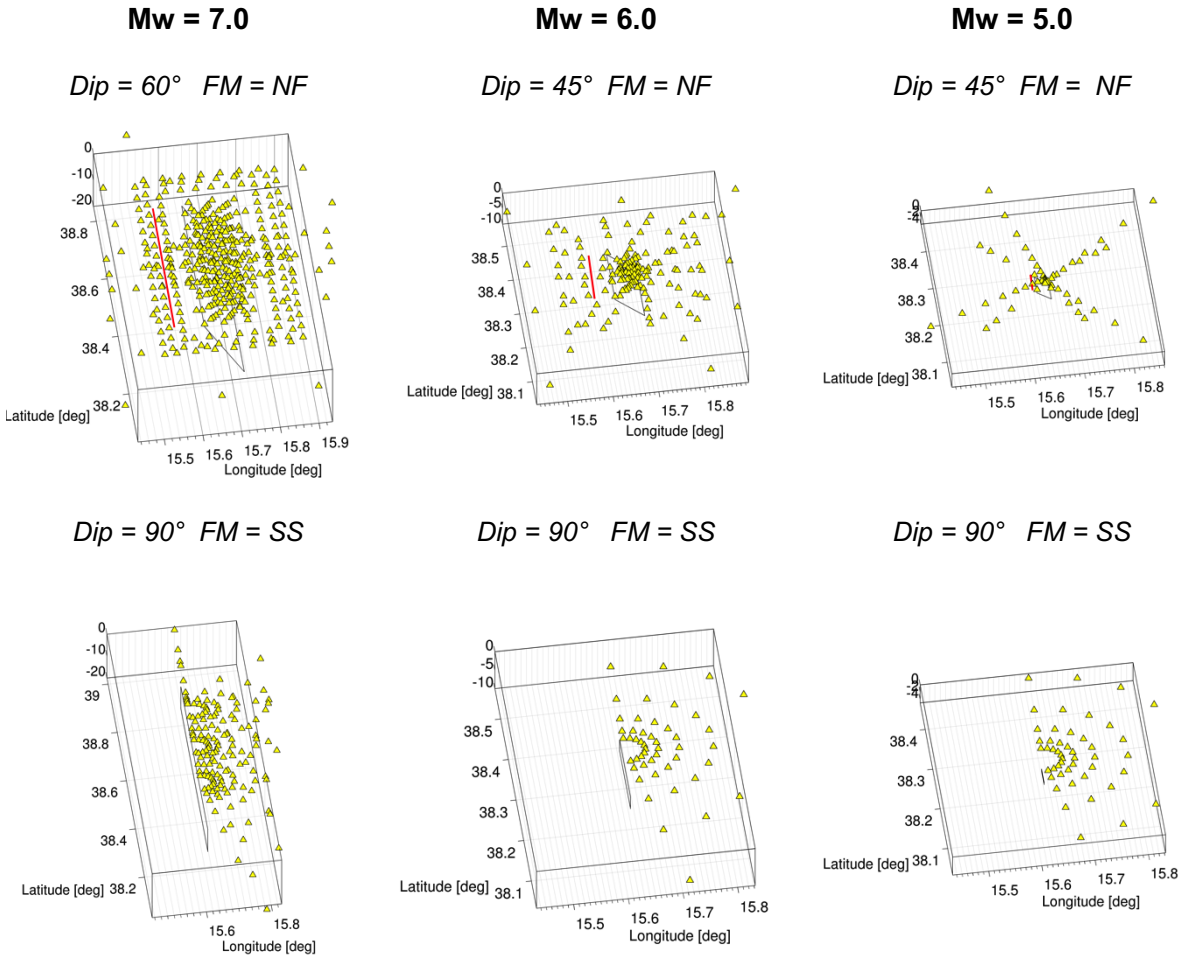

Figure 10 Examples of simulation sites distribution for different magnitudes (Mw = 7.0, 6.0, 5.0) and style of faulting; NF = normal fault; SS = strike-slip fault.

In case of CSS simulations, we generate a set of 3 regularly spaced grids of 190 receivers (along longitude and latitude) whit different degree of resolution around the test site of Priolo-Gargallo (Figure 11). The first one (Figure 11a) is characterized by a radius of about 25 km and grid spacing of 5 km, the second one (Figure 11b) extends up to 5 km from the site whit a grid spacing of 1 km. Because the resolution of the CSS grid should be fine enough to describe the surrounding bedrock properties (Vs ~2500 m/s) and to account for the maximum frequency in the simulated ground motion (5 Hz), we carried out the simulations also over a third denser grid with a resolution of 500 m (up to 2.5 km from Priolo-Gargallo).

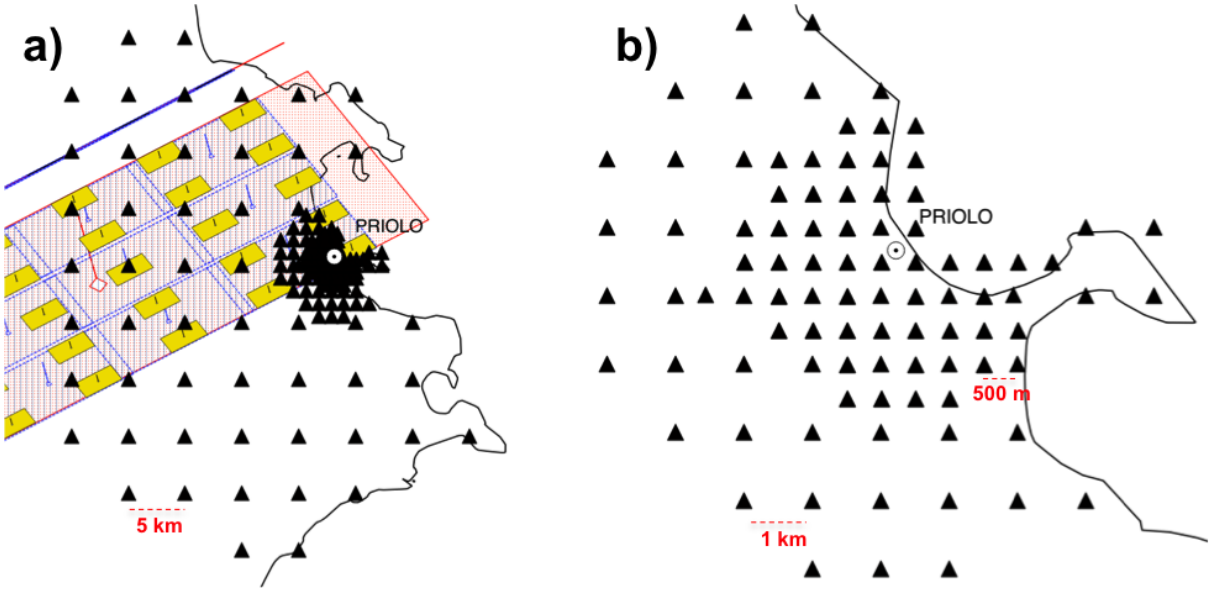

Figure 11 Simulation grids used to simulate the selected composite sources; a) location of the test site for PSHA analysis and grid spacing of the coarsest simulation grid (5 km); b) location of the test site and spacing of the two denser grids (1 km and 500 m, respectively).

Validation exercises

The common approach to address the problem of the reliability of simulations is to validate the modeling again records of past earthquakes (Dreger and Jordan, 2015). A goodness-of-fit between recorded and simulated events is typically given by comparisons of response spectra from simulations with those of selected earthquake. If the resulting goodness-of-fit is unbiased, simulations can be extended to virtual receivers to complete the ground motion field of occurred seismic events. Extending the validation exercise to past earthquakes in different tectonic environments and for wide magnitude-distance ranges, we are confident that the adopted simulations method can be employed to simulate, in a reliable way, future earthquakes. However, this is a sound strategy only when a sufficient number of ground motion recordings is available. In our case a classical goodness-of-fit is very hard to do because strong events are still lacking in the study area. An appropriate alternative would be a model-to-model comparison between simulated ground motion amplitudes and empirical models.

For such reason, we conducted three types of validation exercises:

1. **Comparison between synthetics and GMPEs**: to warranty a simulated ground motion relatively centered on empirical models and to verify if the associated parametric variability can reproduce reasonable ground motion as a whole.

2. **Comparison between synthetics and observed data:** to evaluate the reliability of simulations against past-recorded earthquake; the exercise was driven by one of the major earthquake of the southern Italy of the past 40 years (1978/04/15, Patti Gulf Earthquake Mw=6.0). Some records of the considered event where been compared to GSS simulation outcomes characterized by similar magnitude, focal mechanism, epicentral distance, site class and PGA. The idea is to check whether simulated waveforms well matching recorded ones exist into HPST_db.

3. **Comparison between synthetics and macroseismic data:** to verify the capability of the simulation method to reproduce the intensity field of past earthquakes; the exercise was driven by the same earthquake of exercise n°2, for which a consistent number of macroseismic intensity points is available (CPTI15, Rovida et al., 2016).

Comparison against empirical models

Here we compare the outcomes of the EXSIM simulation set whit preexisting empirical GMPEs. For SMSIM a synthetic vs. empirical model comparison is not meaningful because the simulation magnitudes are out of the validity range of common GMPEs (M_W>= 4.0). The double aim is to examine the variability in the ground motion amplitudes arising from variation in fault rupture kinematics and source-to-site distances and to verify in what measure the adopted simulation method, associated to different degree of variability of the input

parameters, can provide synthetic intensity measures that are consistent with GMPEs calibrated over global, pan-European and regional datasets.

Four models have been selected for comparison:

• CZ14 (Cauzzi et al., 2014) and BSSA14 (Boore et al., 2014), both calibrated over global datasets
• BI14 (Bindi et al., 2014) calibrated over a pan-European dataset
• ITA10 (Bindi et al., 2011) derived from a set of Italian data (1972–2009)

ITA10 still represents the most updated regional model for Italy.

The main characteristics of the GMPEs are listed in Table 9. The GMPEs are heterogeneous in terms of magnitudes, distance, and site conditions. All of them have applicability ranges consistent with the simulated ones. The functional form of BSSA14 was applied without considering basin depth and shear-wave velocity and the basin depth correction is set to zero, as recommended by Boore et al. (2014).

The main tool for evaluating the consistency between simulated data and GMPEs is a single plot for each scenario parameter combination (Figures 12a, 12b, and 12c). Solid black line shows the average of the median prediction for the four selected GMPEs; dotted gray lines were calculated considering the upper and lower bounds of the GMPEs predictions for the four models; grey circles are for a single combination of scenario parameters (magnitude, style of faulting, dip angle, depth of the fault, rupture velocity, k0, and stress parameters) and for a set of ground motion parameters (PGA, SA at 0.3, 1.0, and 3.3 Hz). An acceptance criterion was established to discriminate what scenarios are out of a satisfactory confidence interval that depends on median prediction and standard deviation of each GMPEs. We judged as “well-confident” with empirical models the scenarios for which at least the 80% of samples (simulated ground motion) follow within the boundary of the propagated standard deviation (grey lines) for all selected ground motion parameters.

Table 9
Characteristics of the Candidate Ground-Motion Prediction Equations

Name	Region	Magnitude Type	Magnitude Range	Period (s)	Distance Type	Distance (km)	Site Condition	Style of faulting	Depth (km)	IMs	Component
BSSA14	Global	M_W	3.0 – 8.5	0.01 - 10	Joyner-Boore	0 - 400	VS,30	N,R/T,S, U	0 - 30	PGA, PGV, PSA	RotD50
CZ14	Global	M_W	4.5 - 7.9	0 - 10	Rupture	0-150	EC8 Class/VS, 30	N,R,S,U	0-23	PGA, PGV, DRS	GEOH
BI14	Pan European	M_W-M_L	4.0 - 7.6	0.02 - 3	Joyner-Boore/ Epicentral	0-300	EC8 Class	N,R/T,S, U	0-35	PGA, PGV, PSA	GEOH
ITA10	Regional (Italy)	M_W- M_L	4.0 - 6.9	0.04 - 2	Joyner-Boore/ Epicentral	0-200	EC8 Class	N,R/T,S, U	0-29	PGA, PGV, PSA	GEOH, Z

BSSA14 (Boore et al., 2014); **CZ14** (Cauzzi et al., 2014); **BI14** (Bindi et al., 2014); **ITA10** (Bindi et al., 2011); MW: moment magnitude; ML: local magnitude; EC8 Class: definition of site class based on EC8 code; VS,30: direct use of the shear velocity averaged over the upper 30 m in the equation; N: normal fault; R: reverse fault; T: thrust fault; S: strike fault; U: Unknown; PGA: Peak Ground Acceleration; PGV: Peak Ground Velocity; PSA: Pseudo Spectral Acceleration; PSV: Pseudo Spectral Velocity; IA: Arias Intensity; IH: Housner Intensity; DV: Strong motion Duration; GEOH: geometric mean of horizontal components; H: maximum amplitude of horizontal components; Z: vertical component; RotD50: median single-component horizontal ground motion across all non-redundant azimuths.

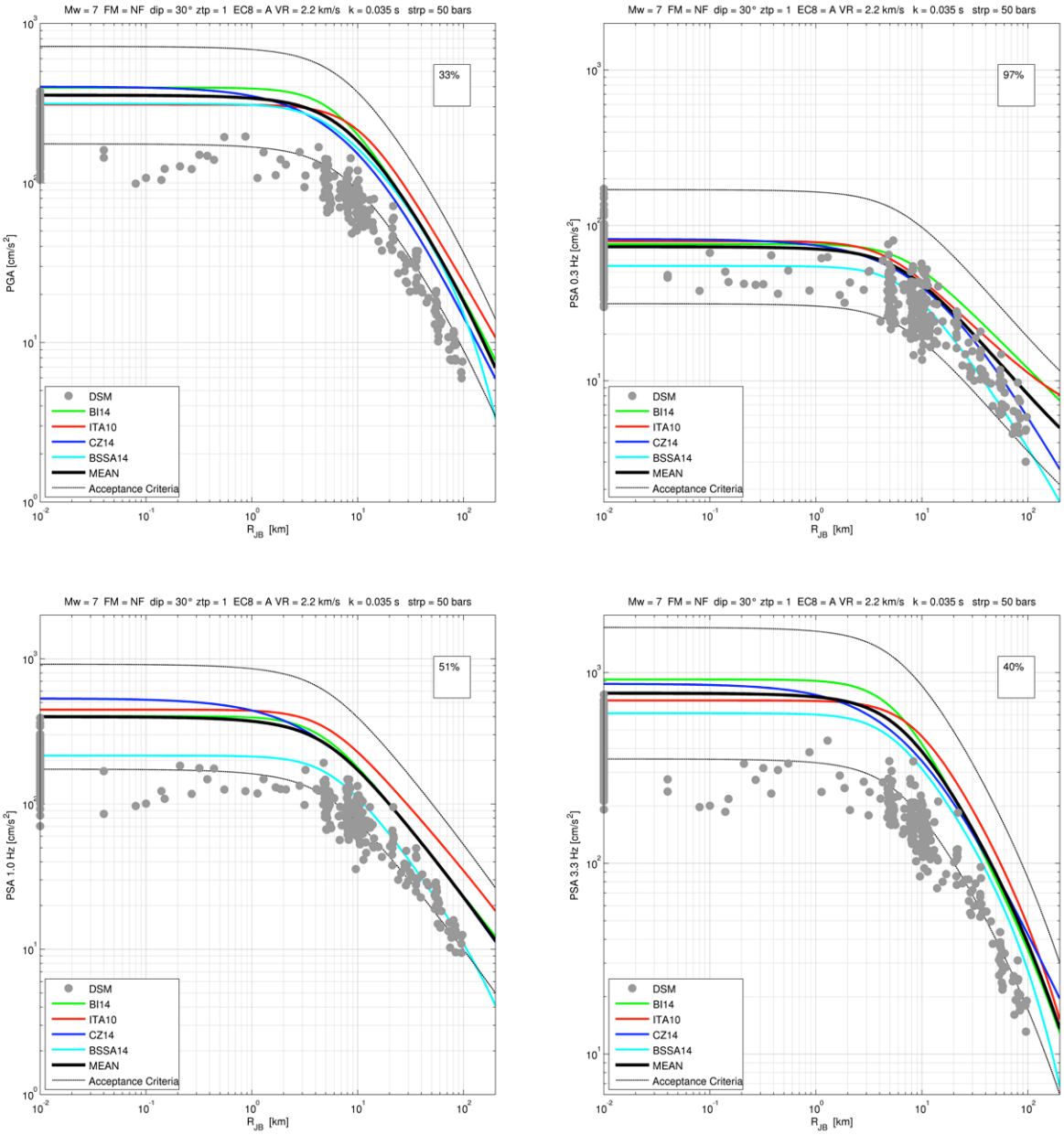

Figure 12a Exemplum of validation exercise comparing PGA, PSA at 0.3, 1.0, and 3.3 Hz for a M7.0 scenario event (see title figure for combination parameters) against ground motion prediction equations. The GMPEs are BSSA14 (Boore et al., 2014), CZ14 (Cauzzi et al., 2014), BI14 (Bindi et al., 2014), and ITA10 (Bindi et al., 2011). Black line: average of the median prediction from the four GMPEs; dotted gray line: confidence interval calculated considering the upper and lower bounds of the GMPEs predictions for the four models; grey circles: single combination of DSM scenario parameters.

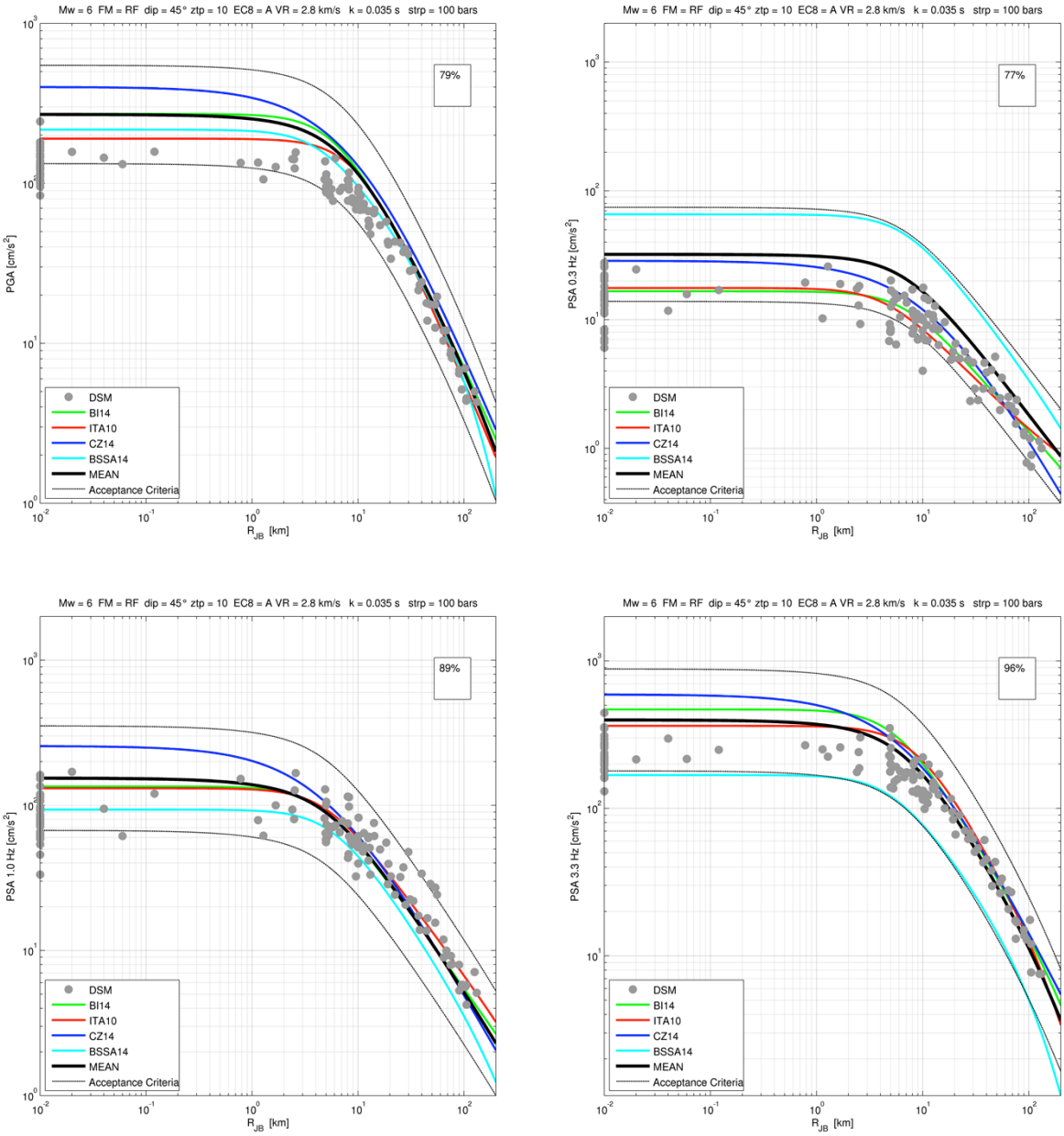

Figure 12b Exemplum of validation exercise comparing PGA, PSA at 0.3, 1.0, and 3.3 Hz for a M6.0 scenario event (see title figure for scenario parameters) against ground motion prediction equations. The GMPEs are BSSA14 (Boore et al., 2014), CZ14 (Cauzzi et al., 2014), BI14 (Bindi et al., 2014), and ITA10 (Bindi et al., 2011). Black line: average of the median prediction from the four GMPEs; dotted gray line: confidence interval calculated considering the upper and lower bounds of the GMPEs predictions for the four models; grey circles: single combination of DSM scenario parameters.

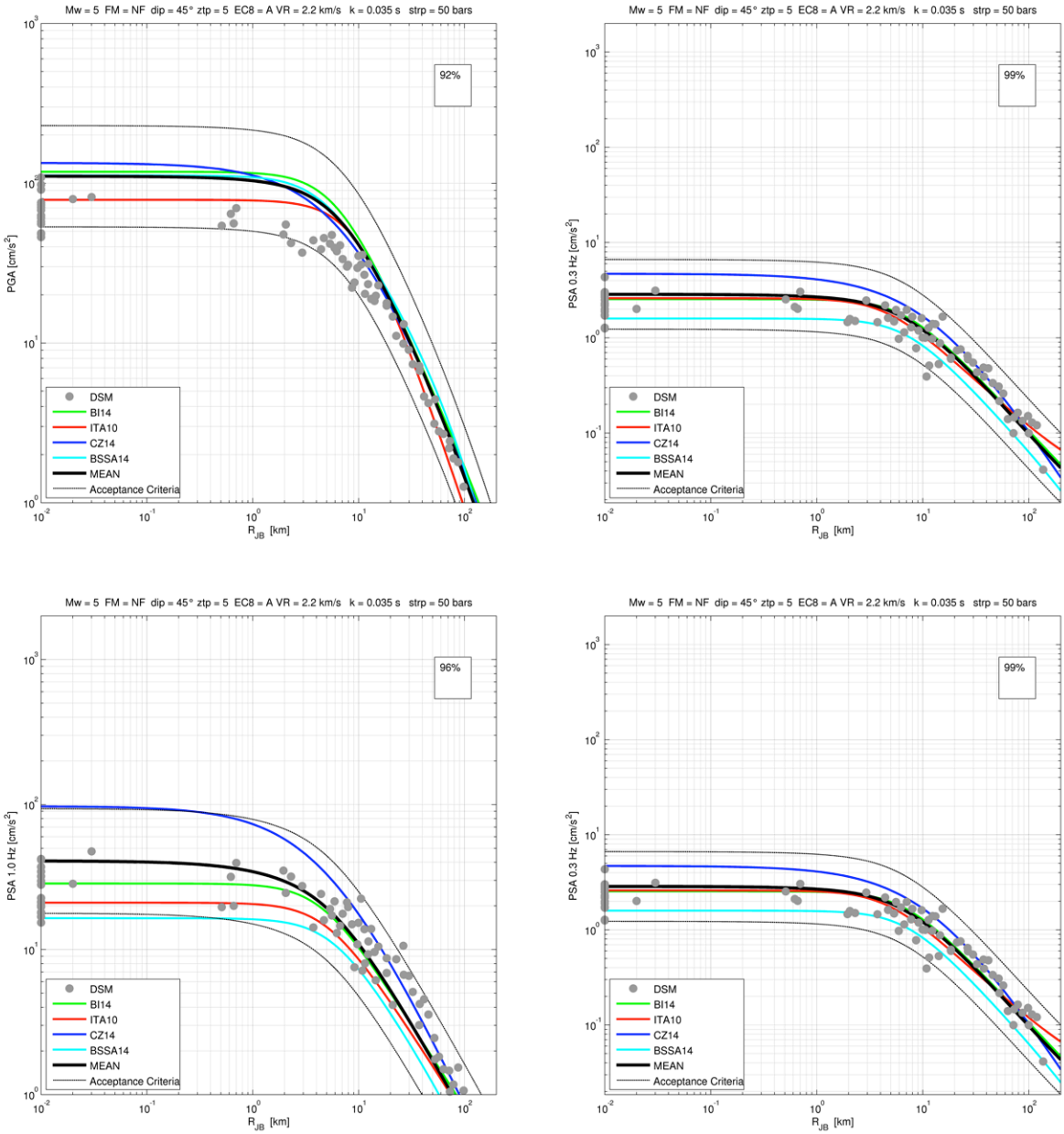

Figure 12c Exemplum of validation exercise comparing PGA, PSA at 0.3, 1.0, and 3.3 Hz for a M5.0 scenario event (see title figure for scenario parameters) against ground motion prediction equations. The GMPEs are BSSA14 (Boore et al., 2014), CZ14 (Cauzzi et al., 2014), BI14 (Bindi et al., 2014), and ITA10 (Bindi et al., 2011). Black line: average of the median prediction from the four GMPEs; dotted gray line: confidence interval calculated considering the upper and lower bounds of the GMPEs predictions for the four models; grey circles: single combination of DSM scenario parameters.

Comparison against observed data

The main objective of the Task2 of the projects is to provide a comprehensive synthetic dataset that could be representative not only to past events but also to future earthquakes. As already observed, the low level of seismicity in the understudy area make very hard to do a classical goodness-of-fit between recorded and synthetic data. Only three earthquakes whit moment magnitude greater than 5.5 and hypocentral depth less that 30 km are available in the ITACA database (1978/04/15 Patti Gulf, Mw=6.0; 2002/09/06 Palermo, Mw=5.8; 1990/12/13 Southern-East Sicily, Mw=5.6; http://itaca.mi.ingv.it). All of them were recorded in offshore and are characterized by very few records at epicentral distances larger than 10 km. Moreover, recorded data include site effects, whereas simulated data have been performed for very hard rock site conditions (Vs30>2000 m/s). A direct comparison between recorded data and synthetic ones is thus impossible.

In this section we attempt to retrieve, within the bulk of simulated waveforms, synthetic data compatible with recorded ones. As benchmarks we have chosen three records of the Mw=6.0 Patti Gulf earthquake: IT.GRR, IT.NAS, and IT.MSS1. Metadata and peak parameters related to recording stations (network code, station code, station coordinates, EC8 soil category, epicentral distance, backazimut to the epicenter, and peak parameters) are summarized in Table 10.

Table 10

Metadata and peak parameters of the selected stations recording the 1978 Mw=6.0 Patti Gulf earthquake

Network Code	Station Code	Lon [°]	Lat [°]	EC8	R_{epi} [km]	BKZ [°]	PGA [cm/s^2]	PGV [cm/s]	PGD [cm]
IT	NAS	14.78630	38.11840	C	33.0	59.2	145.245	8.162	0.754
IT	MSS1	15.51583	38.20694	B*	36.2	281.3	37.149	2.057	0.227
IT	GRR	15.16278	37.72611	A*	60.5	355.6	28.356	3.152	0.443

IT: Italian Strong Motion Network managed by Department of the Civil Protection; EC8: eurocode8 classification (soil categories marked by * are attributed on the base of surface geology); R_{epi}: epicentral distance; BKZ: back azimuth respect to epicenter. Peak parameters (PGA, PGV and PGD) are for the geometrical mean of the two-horizontal component of the ground motion (NS and EW).

IT.NAS is the only station well characterized from the geophysical and geotechnical point of view (DPC-INGV-S2-2014, https://goo.gl/qknCJs). It follows in C class with an average share wave velocity within 30 m (Vs30) of 291 m/s and an average Vs to the bedrock of 502 m/s. Station IT.MSS1 and IT.GRR follows in EC8 class B* and A*, respectively.

For each record of Table 10, we went looking for those synthetics in HYPST_dtb able to reproduce some aspects of the recorded waveforms. Firstly, we considered synthetics characterized by Mw=6.0, strike-slip style of faulting, and hypocentral depth (+/- 5 km)

associated to epicentral distance (+/- 5 km) similar to each selected record. After that, we simulated again the synthetics applying amplification factors for the Fourier spectrum that are specific for the soil condition of the recording stations. The only exception is for IT.GRR being recorded at the bedrock (EC8=A*). In this case we selected the suite of synthetics also on the base of the recorded PGA (+/- 5 cm/s^2). Amplification factors are from Boore and Joyner (1997) and are reported in Tables 11 for generic very hard rock site (Vs30=2900 m/s), generic rock site (Vs30=620 m/s) and generic soil (Vs30=310 m/s).

Table 11

Amplification factors for Generic Very Hard Rock Site, Generic Rock Site and Generic Soil

(Boore and Joyner, 1997)

Frequency [Hz]	Amplification Vs30=2900 m/s (Generic Very Hard Rock Site)	Frequency [Hz]	Amplification Vs30=620 m/s (Generic Rock Site)	Amplification Vs30=310 m/s (Generic Soil)
0.01	1.00	0.01	1.00	1.00
0.10	1.02	0.09	1.10	1.34
0.20	1.03	0.16	1.18	1.57
0.30	1.05	0.51	1.42	2.24
0.50	1.07	0.84	1.58	2.57
0.90	1.09	1.25	1.74	2.76
1.25	1.11	2.26	2.06	2.98
1.80	1.12	3.17	2.25	2.95
3.00	1.13	6.05	2.58	3.05
5.30	1.14	16.60	3.13	3.18
10.00	1.15	61.20	4.00	3.21

Figures 13, 14 and 15 reports station locations, Husid plots (integral of the Arias Intensity) and some examples of synthetics well matching the recorded ones. Husid plots are produced to allow a visual assessment of the energy release with time, while plots of simulated waveform laid on s-wave phase of records provide a first-order verification that synthetics are reasonable (Goulet et al., 2015).

For IT.GRR, according to the search criteria described above, we found 13 possible correspondences between synthetics and observed waveforms. Even if IT.GGR station is far from the source (R_{epi}=60.5 km, see Figure 13a), the integrals of the Arias intensity (Figure 13b) are within a narrow band (blue lines) showing a trend similar to those observed for the horizontal component (s-phase) of the motion (black lines). It ensures a good correspondence in terms of energy release in time. As regards the comparison between simulated (red lines) and recorded waveforms (black lines), it should be noted that synthetics are well matching between the first 10-12 s of the signal, but much longer durations were been simulated for the s-phases of the motion (Figure 13c,d).

For IT.NAS and IT.MSS1 we found, obviously, a major number of correspondences (360 and 303 respectively) because the synthetic PGAs have not been constrained. In case of IT.NAS (Figure 14b) the energy release in time extends over a large band showing that selected synthetic waveforms are very heterogeneous in terms of duration and amplitude of the motion. For IT.MSS1 we generally observe that the main energy release of synthetics is confined in time intervals of half duration of observed s-phases. However, it was possible discriminate (both for IT.NAS and IT.MSS1) at least a pair of synthetics that reproduce in a satisfactory way the observed ground motion in terms of amplitude, duration and frequency content of the recorded motion (Figures 14b,c and Figures 15b,c).

a)

b)

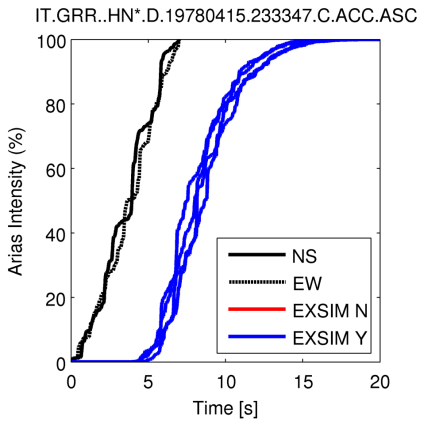

c)

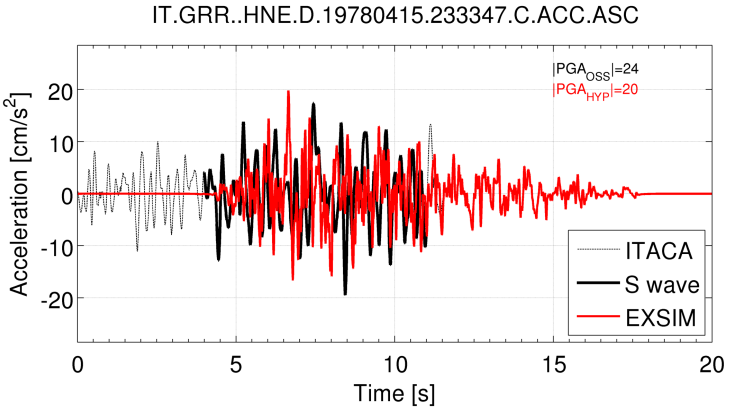

d)

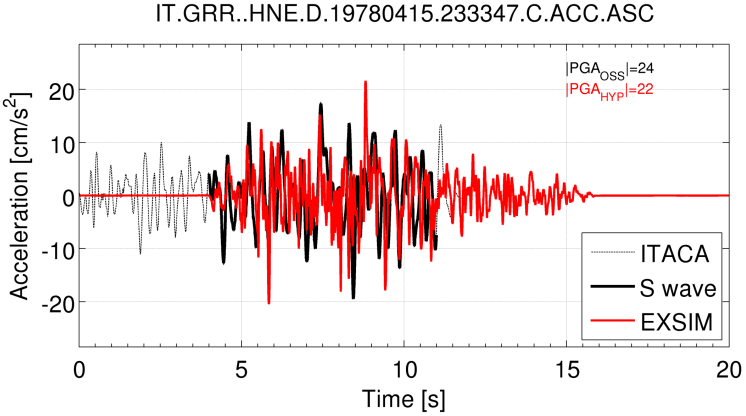

Figure 13 Examples of output produced by validation exercise again recorded data; a) location of the IT.NAS (EC8 A*) recording the benchmark earthquake (1978 Patti Gulf, Mw=6.0); b) Integral of Arias intensity for a set of realizations from HYPST_dtb dataset compared to observations (black line: NS recorded component; black dotted line: EW recorded component; blue lines: well matching simulated data; red lines: poor matching simulated data); c-d) examples of two acceleration time series extracted from HYPST_dtb matching the recorded waveform (EW component) of the IT.NAS station (black dotted line: full waveforms from ITACA archive http://itaca.mi.ingv.it/, black line: S-wave time windows; red line: simulated data).

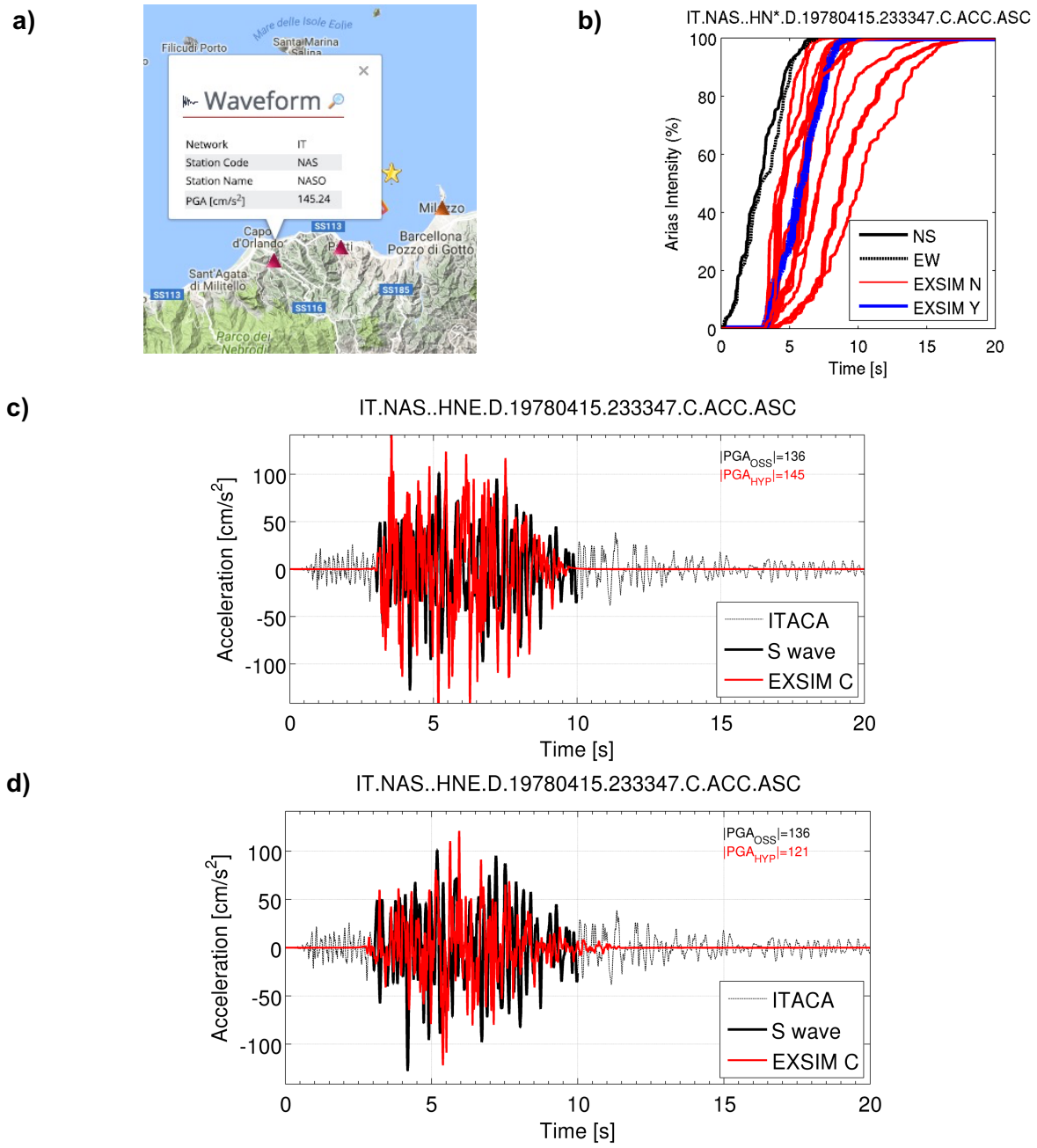

Figure 14 Examples of output produced by validation exercise again recorded data; a) location of the IT.NAS (EC8 C) recording the benchmark earthquake (1978 Patti Gulf, Mw=6.0); b) Integral of Arias intensity for a set of realizations from HYPST_dtb dataset compared to observations (black line: NS recorded component; black dotted line: EW recorded component; blue lines: well matching simulated data; red lines: poor matching simulated data); c-d) examples of two acceleration time series extracted from HYPST_dtb matching the recorded waveform (EW component) of the IT.GRR station (black dotted line: full waveforms from ITACA archive http://itaca.mi.ingv.it/, black line: S-wave time windows; red line: simulated data).

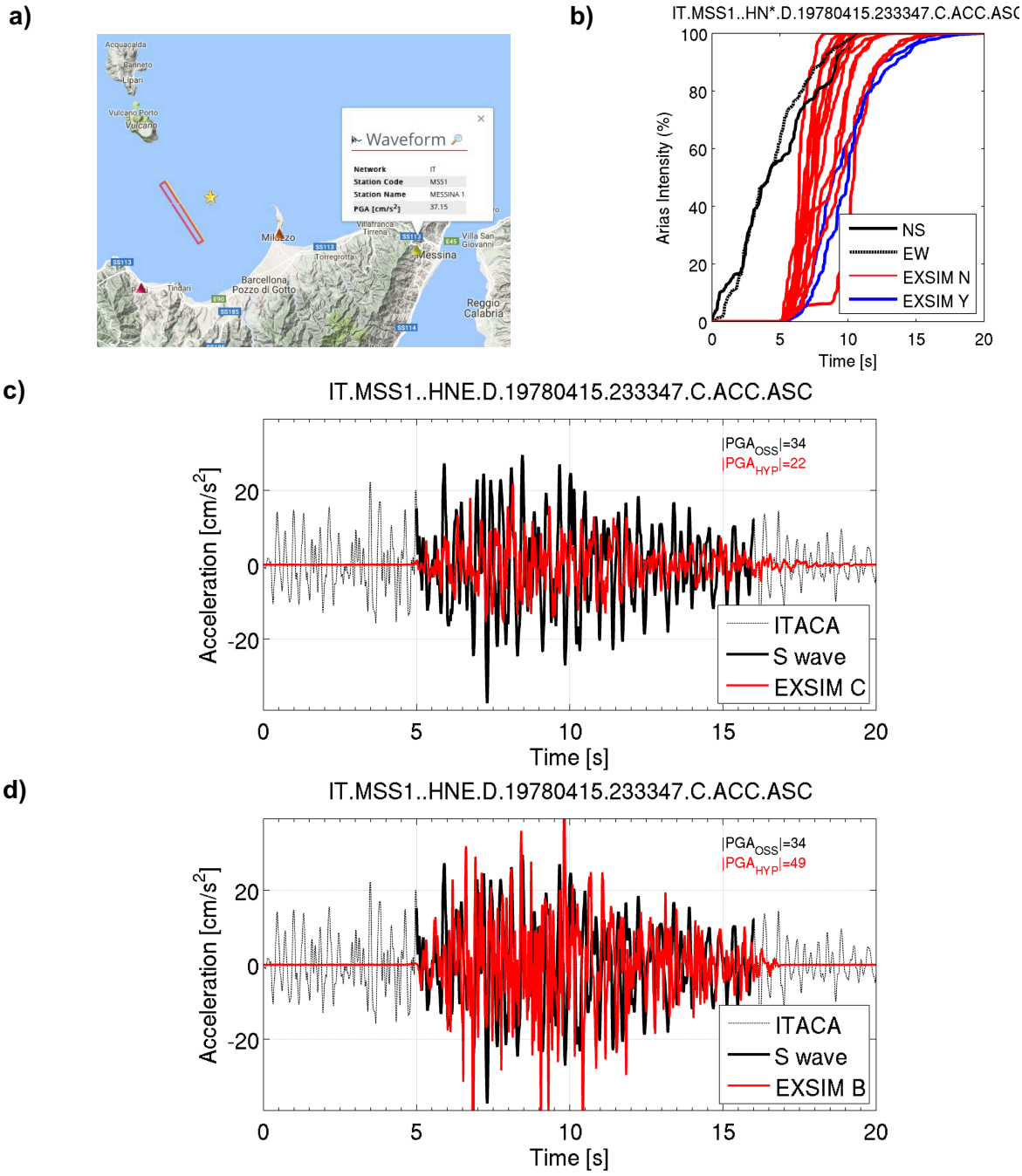

Figure 15 Examples of output produced by validation exercise again recorded data; a) location of the IT.MSS1 (EC8 B*) recording the benchmark earthquake (1978 Patti Gulf, Mw=6.0); b) Integral of Arias intensity for a set of realizations from HYPST_dtb dataset compared to observations (black line: NS recorded component; black dotted line: EW recorded component; blue lines: well matching simulated data; red lines: poor matching simulated data); c-d) examples of two acceleration time series extracted from HYPST_dtb matching the recorded waveform (EW component) of the IT.MSS1 station (black dotted line: full waveforms from ITACA archive http://itaca.mi.ingv.it/, black line: S-wave time windows; red line: simulated data).

Comparison against macroseismic data

To verify the capability of the simulation method to reproduce the intensity field of past earthquakes we considered one of the major earthquakes of the southern Italy of the past 40 years (1978/04/15, Patti Gulf Earthquake Mw=6.0; CPTI15, Rovida et al., 2015) for which a consistent number of macroseismic intensity points is available (Figure 16; DBMI15, Locati et al., 2016). We simulated the 1978 event considering the source geometry proposed by the DISS (https://goo.gl/hhrxgx). We considered the same quality factor and geometrical spreading already used to generate scenarios both for generic and composite sources (D'Amico 2010), together with a random slip distribution. Other main simulation parameters are reported in Table 12. Each site of the macroseismic intensity field was previously classified as Generic Very Hard Rock Site (Vs30=2900 m/s), Generic Rock Site (Vs30=620 m/s) or Generic Soil (Vs30=310 m/s), hence we simulated synthetic acceleration time series applying amplification factors for the Fourier spectrum that are specific for the soil condition (Table 11).

Table 12

Modeling parameters for the simulation of the 1978 Patti Gulf earthquake

Parameter	Value
Strike, Dip, Rake [°]	147, 83, 180
Depth of the upper left corner [km]	1.5
Shear-wave velocity [km/s] (β)	3.3
Density [g/cm3]	2.66
Rupture propagation speed [km/s] (Vr)	0.85 (x β)
Kappa [s]	0.035
Stress parameter [bar]	50
Number of iterations over hypocenter	10

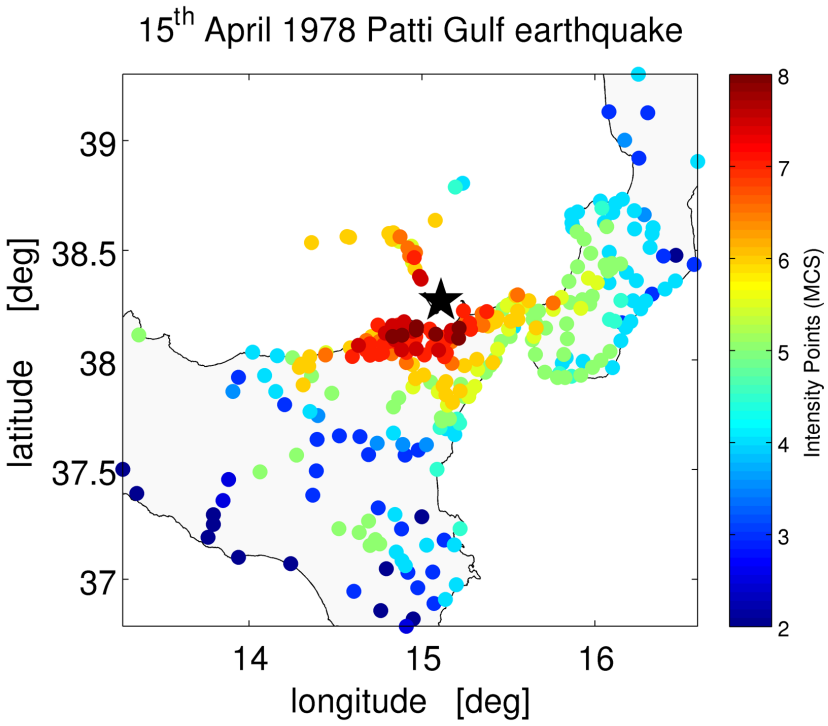

Figure 16 Intensity points of the Mw=6.0, 1978 Patti Gulf earthquake; DBMI15, Locati et al., 2016.

Figure 17 shows the PGAs distribution simulated by EXSIM in correspondence of the intensity points of the 1978 earthquake (Figure 16) compared to those obtained by using three different relationships between macroseismic intensity and PGA (GOMAL: Gomez et al., 2018 in Appendix; FAEMI10: Faenza and Michelini, 2010; MAR992: Margottini et al., 1992).
We observe that the PGAs distribution obtained by EXSIM for different soil conditions (hard rock, stiff and soft soil) agrees with those provided by GOMAL and MAR992 only for epicentral distances less than 50 km, whereas, for greater distances, the simulated values are considerably lower (Figure 18). The best agreement can be observed between synthetic data and PGAs obtained by FAEMI10 within the whole range of distance (Figure 18).

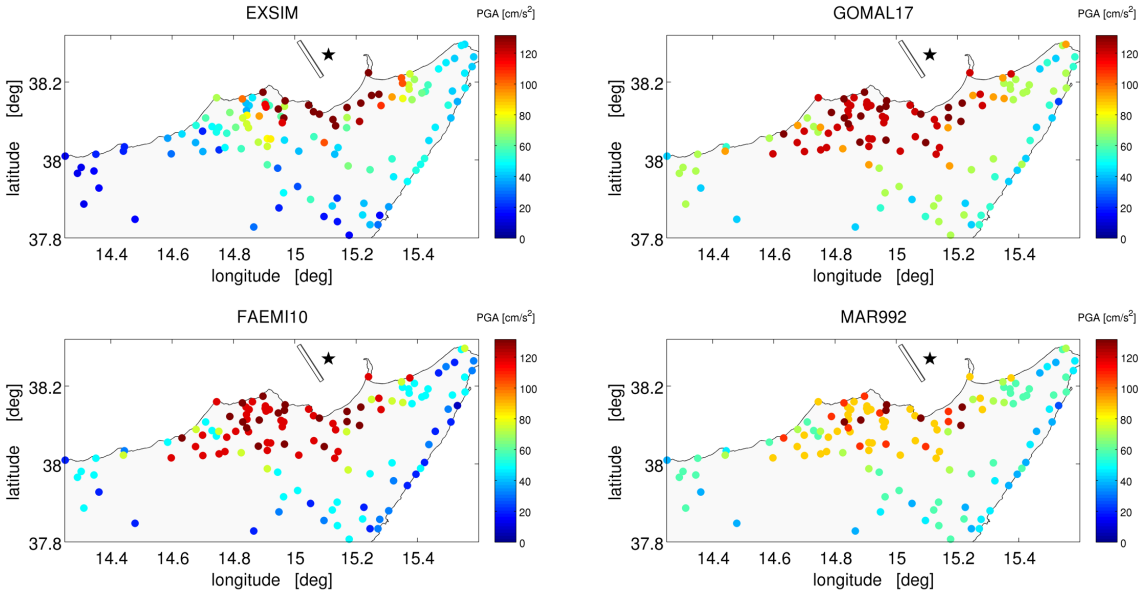

Figure 17 1978 Patti Gulf earthquake scenarios (geometrical mean of the horizontal components) performed by EXSIM or applying to the intensity point distribution three different empirical relations between macroseismic data and PGAs (GOMAL: Gomez et al., 2018 in Appendix; FAEMI10: Faenza and Michelini, 2010; MAR992: Margottini et al., 1992).

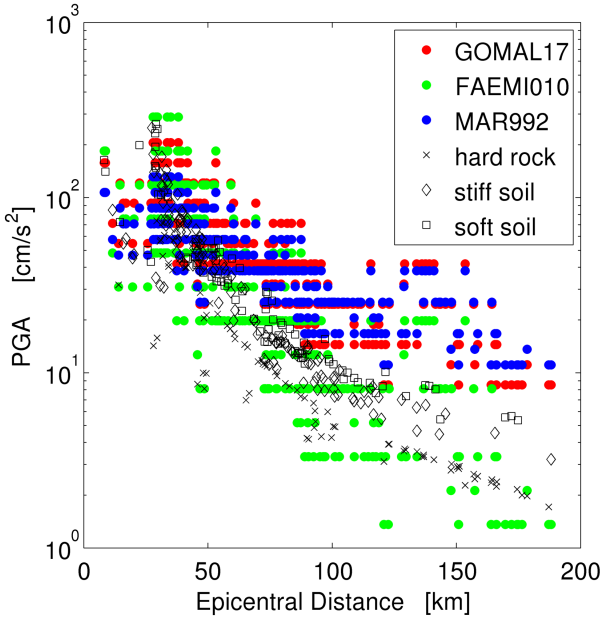

Figure 18 Comparison between 1978 Patti Gulf earthquake scenarios (PGAs vs Epicentral distance) obtained by using a set of relations between macroseismic intensity and PGA (GOMAL, Gomez et al., 2018 in Appendix; FAEMI10, Faenza e Michelini, 2010; MAR992, Margottini et al., 1992) and simulated by EXSIM for different soil categories (hard rock, stiff and soft soil).

Synthetic dataset

Data description

The synthetic dataset (HYPST_dtb) encompasses more than 180,000 strong motion data. Figure 19 reports the magnitude-distance distribution of both simulated (GS: red circle; PLS: blue circle) and empirical data from Task 1 (grey circle) together with histograms of style of faulting, magnitude and distance for the GS synthetic dataset. About 1/3 of the data are relative to magnitude larger than 7.0; more than half of the dataset are composed by waveforms of receivers located in the distance range 0-25km. Finally, the dataset is mainly composed by normal and reverse events, rather than strike-slip ones.
Figure 20 shows an exemplum of synthetic ground motion attenuation in function of the Joyner-Boore distance for all simulated magnitudes (Mw = 3.5; 4.0; 4.5; 5.0; 5.5; 6.0; 6.5; 7.0; 7.5); in this case only normal faults were considered. Synthetic median is sampled through binned white dots in order to compile attenuation tables in the mandatory format required by CRISIS2015 for further computation of seismic hazard (see Task4 deliverable).
Figures 21a, 21b, and 21c show the distribution of PGA, SA at 0.3s, 1s and 3s for the synthetic GSs data at magnitude 5.0, 6.0, and 7.0, respectively. The data follow quite well a lognormal distribution. The values of the total standard deviation (in decimal logarithm units) of the synthetic data are reported in Table 14, compared to those proposed by the most recent ground motion for Italy (ITA10, Bindi et al., 2011). The sigma's obtained by the simulations are larger than the empirical ones, especially at lower magnitudes. In Tables 15a, 15b, and 15c, we also report median and sigma values for different style of faulting.
To investigates how the parametric variability due to different input simulations contribute to the ground motion variability, Figures 22-24 show the synthetic cumulative distribution functions (CDFs) of PGA computed for all simulated magnitudes and related to the variation in style of faulting (Fig 22), and depth of the fault (Fig 23), stress parameter (Fig 24). No significant changes from the overall distributions are observed for different styles of faulting for all magnitudes. Regarding to the depth of the fault, as the magnitude increases the variability decreases, showing as larger uncertainties in the source position for lower magnitudes produces a larger variability of the ground motion. The most significant contribution derives from variability on the kinematic process over the fault (rupture velocity combined with random sample of the nucleation points) and stress parameter.

Flat-files

The HYPST_dtb is composed by two flat-files related to generic sources modeled by EXSIM (GS_DTB) or SMSIM (PLS_DTB). Table 13 describes the fields contained in the GS_DTB. Like to the empirical dataset (see Task1 deliverable), the metadata are grouped in three main categories related to stations (e.g. location of the simulation sites, soil classification), scenario events (e.g. scenario event ID, fault mechanism, location of the simulated event, magnitude, simulation grid), and ground motion parameters (geometrical mean of the horizontal component of PGA, PGV, and PSA at 0.3, 1, and 3 s). Additional fields were introduced to account: i) virtual receivers located in the hanging wall or footwall of the fault (hw_fw); ii)

scenario parameters satisfying the acceptance criteria established in the previous section of the report (prct_flag).

Table 13 Description of the fields contained in the GS_DTB

Field name	Description	Example
file_name	Name of the output file generated by EXSIM	*GAF_M_5_0_S_1_distances_psa.out*
scen_eve_id	Univocal scenario event ID	*HPST_501*
es_strike	Strike of the fault [deg]	*0*
es_dip	Dip of the fault [deg]	*90*
es_z_top	Depth of the top of the fault [km]	*5*
fm_type_code	Focal mechanism	*S*
ev_latitude	Latitude of the simulated event [deg]	*38.2599*
ev_longitude	Longitude of the simulated event [deg]	*15.6322*
ev_depth_m	Depth of the simulated event [km]	*7*
Mw	Moment magnitude	*5*
net_code	String to identify the simulation grid	*HPST_5_1*
station_code	Alphanumerical code to identify the simulation site	*S1*
st_latitude	Latitude of the simulation site [deg]	*38.279*
st_longitude	Longitude of the simulation site [deg]	*15.633*
vs30_m_sec	Average shear-wave velocity to 30m depth [m/s]	*2000*
ec8_code	EC8 site classification	*A*
epi_dist	Epicentral distance [km]	*2.1202*
epi_az	Azimuth of the simulation site respect to the epicenter	*1.9205*
JB_dist	Joiner an Boore distance [km]	*1.27*
rup_dist	Rupture distance [km]	*5.16*
vrup	Rupture velocity [km/s]	*2.2*
stress	Stress parameter [bars]	*50*
kappa	Kappa factor [s]	*0.035*
e_hp	High pass cut-off frequency for the EW component [Hz]	*0.01*
n_hp	High pass cut-off frequency for the NS component [Hz]	*0.01*
e_lp	Low pass cut-off frequency for the EW component [Hz]	*25*
n_lp	Low pass cut-off frequency for the NS component [Hz]	*25*

gm_pga	Geometrical mean of the PGA horizontal components [cm/s^2]	*62.22*
gm_pgv	Geometrical mean of the PGV horizontal components	*2.633*
gm_T_0_3	Geometrical mean of the SA at 0.3 s horizontal components [cm/s^2]	*91.23*
gm_T_1_0	Geometrical mean of the SA at 1.0 s horizontal components	*20.99*
gm_T_3	Geometrical mean of the SA at 3 s horizontal components [cm/s^2]	*2.645*
az_ref_pnt	Azimuth of the simulation site respect to the UL corner of the fault [deg]	*0.7952*
hw_fw	Flag to identify if the simulation site is located in the hanging wall or the footwall (1: hanging wall; 2: footwall)	*1*
prct_flag	Flag to identify is the simulated event satisfies the acceptance criteria given by the 80% of ground motion values (PGA, SA at 0.3, 1.0, 3.3 s) within the boundary of the propagated standard deviations of a set of reference GMPEs (1: well-confident; 0: not-confident).	*0*

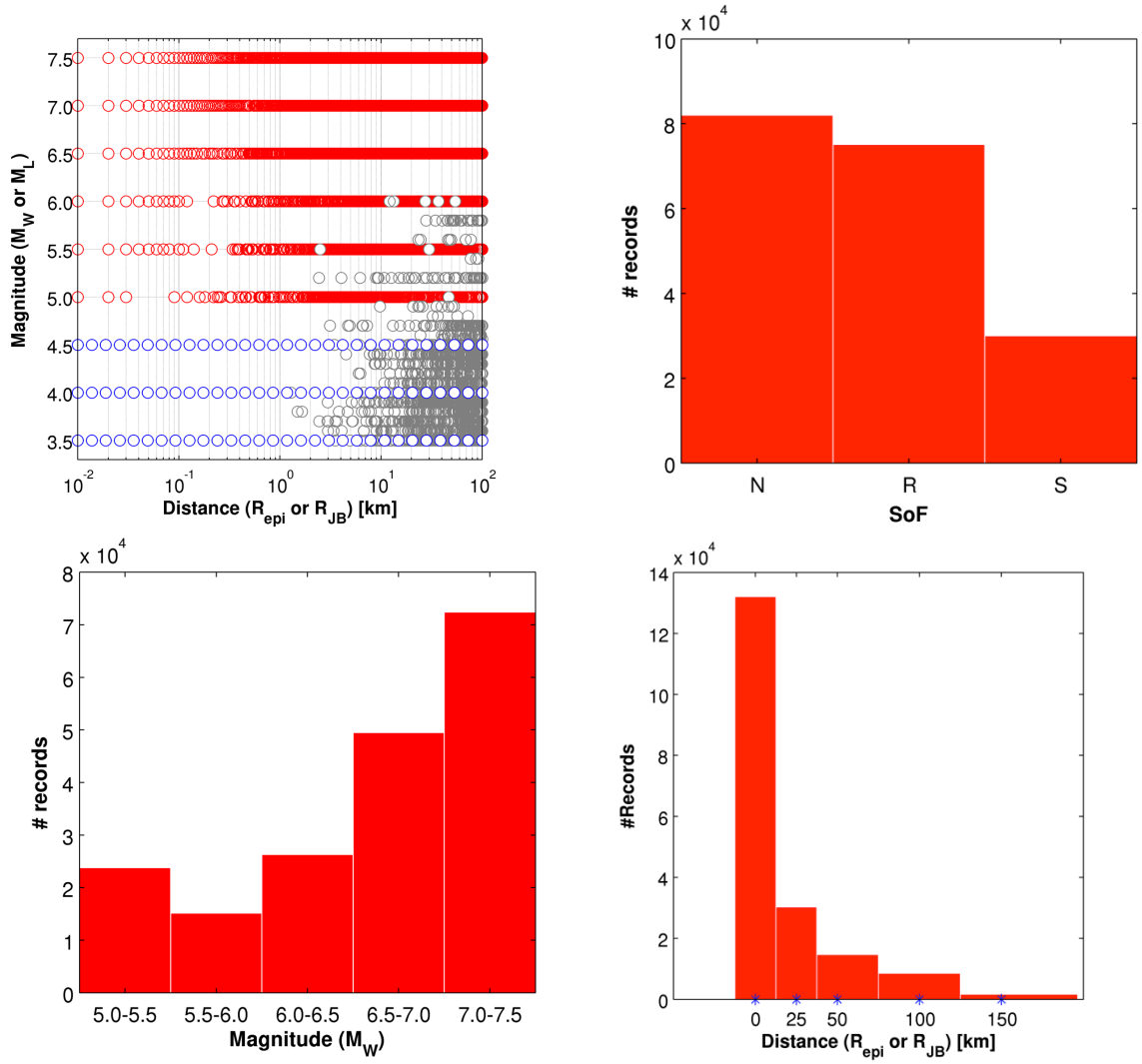

Fig 19 Magnitude (M_W or M_L) versus distance distribution of empirical (grey circle) and synthetic (GS: red circle; PLS: blue circle) flat-file (a); distribution of simulated waveforms in function of (b) style of faulting (N: normal faults; R: reverse faults; S: strike-slip faults); (c) magnitude bins; (d) fault-to-site distance.

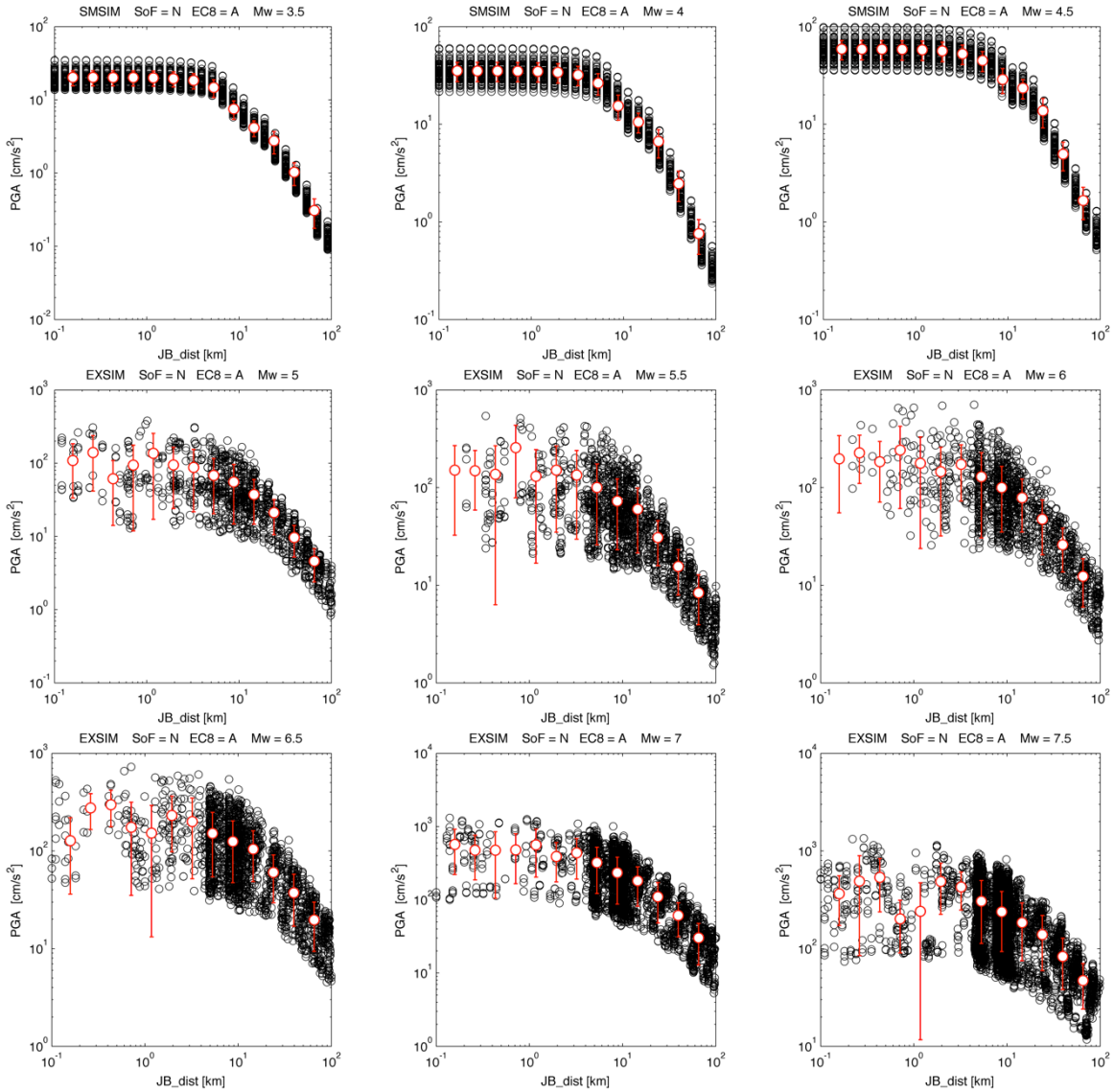

Fig 20 Synthetic PGAs vs fault distance (R_{JB}) for hard rock sites (NEHRP A, Vs>=2000 m/s), normal faults, and all sampled magnitudes (Mw = 3.5; 4.0; 4.5; 5.0; 5.5; 6.0; 6.5; 7.0; 7.5). White dots and red bars represent the mean value and standard deviation of the simulated ground motion for each distance bin, respectively.

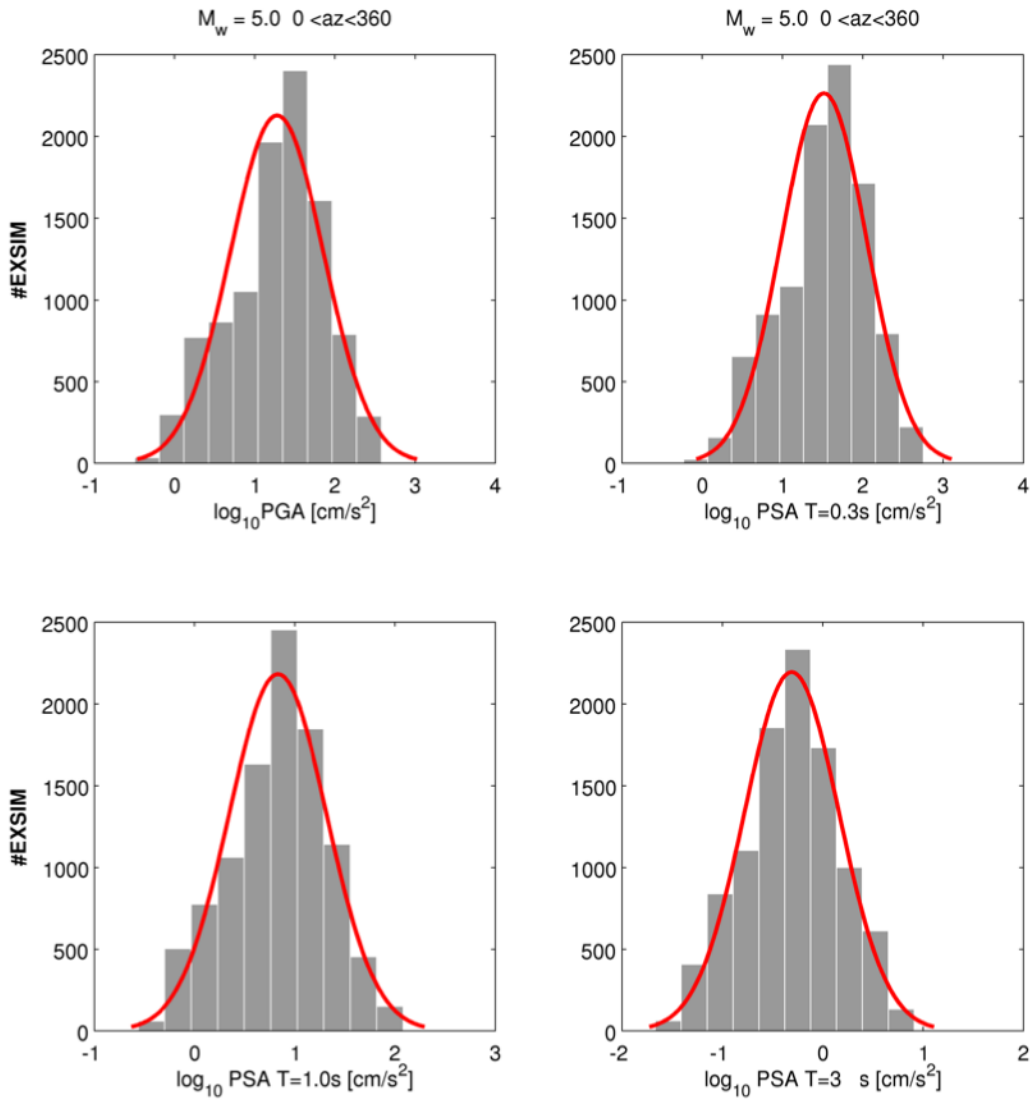

Fig 21a Histograms of synthetic PGAs and PSA at 0.3, 1.0, and 3 s for M5.0, fitted by a normal distribution (red curve). Ground motion values are in log10 units.

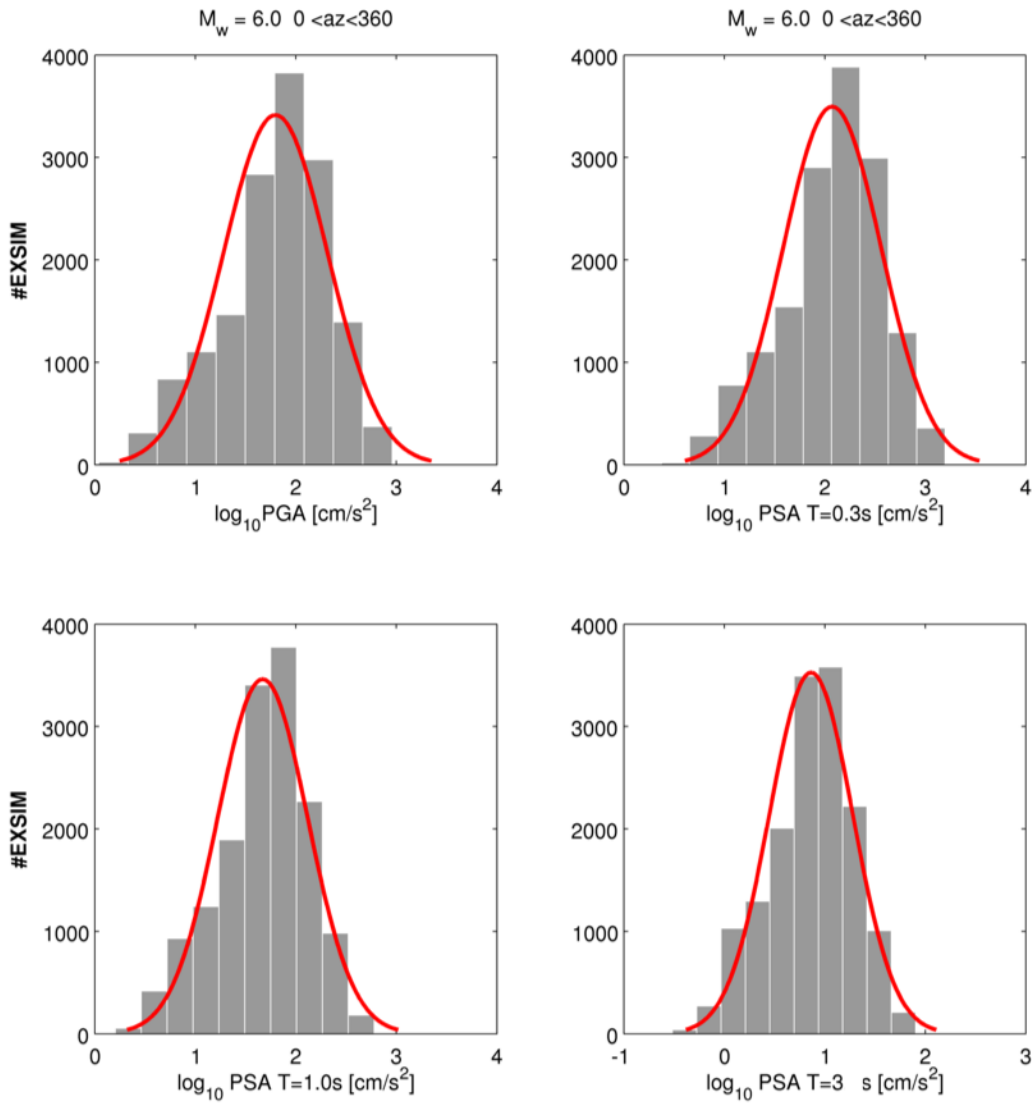

Fig 21b Histograms of synthetic PGAs and PSA at 0.3, 1.0, and 3 s for M6.0, fitted by a normal distribution (red curve). Ground motion values are in log10 units.

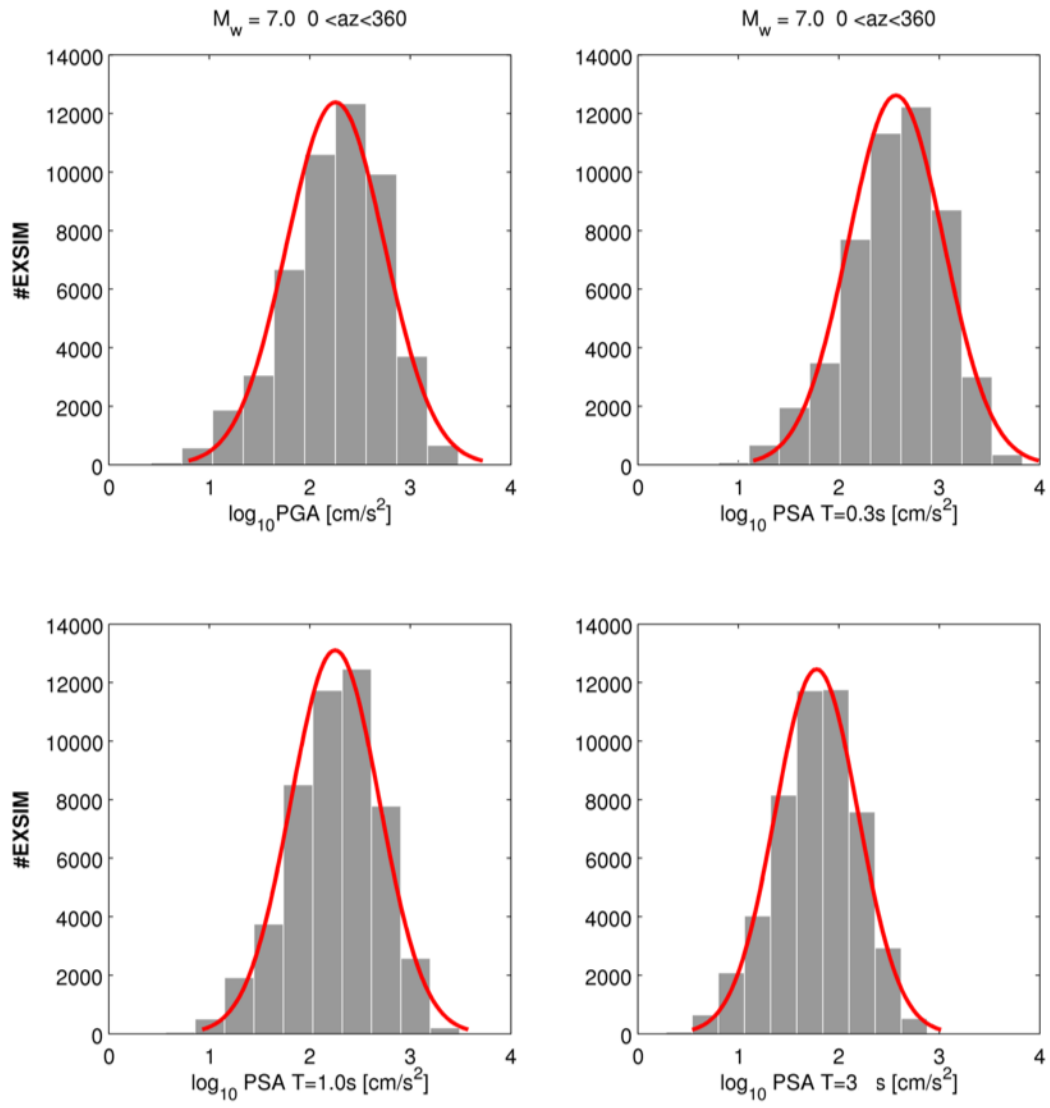

Fig 21c Histograms of synthetic PGAs and PSA at 0.3, 1.0, and 3 s for M7.0, fitted by a normal distribution (red curve). Ground motion values are in log10 units.

Table 14 Standard deviations of GS dataset

Dataset	PGA	SA=0.3s	SA=1s	SA=3s
M_W 7.5	0.4073	0.3983	0.3791	0.3603
M_W 7.0	0.4871	0.4733	0.4404	0.4123
M_W 6.5	0.4718	0.4525	0.4188	0.3869
M_W 6.0	0.5167	0.4879	0.4491	0.4148
M_W 5.5	0.5505	0.5091	0.4675	0.4466
M_W 5.0	0.5812	0.5297	0.4873	0.4725
ITA10	0.3370	0.3630	0.3600	--

Table 15a Median values and standard deviation for normal fault

GMP	Mw	Median	Standard deviation
PGA	**3.5**	0.63	0.92
	4.0	0.93	0.84
	4.5	1.20	0.79
	5.0	1.40	0.59
	5.5	1.63	0.56
	6.0	1.81	0.50
	6.5	1.96	0.44
	7.0	2.38	0.50
	7.5	2.40	0.41
PSA 0.3 s	**3.5**	0.12	0.61
	4.0	0.60	0.54
	4.5	1.14	0.58
	5.0	1.64	0.54
	5.5	1.89	0.51
	6.0	2.09	0.48
	6.5	2.25	0.43
	7.0	2.67	0.48
	7.5	2.71	0.40
PSA 1.0 s	**3.5**	-0.88	0.57
	4.0	-0.20	0.56
	4.5	0.53	0.59
	5.0	0.96	0.50
	5.5	1.38	0.48
	6.0	1.68	0.43
	6.5	1.92	0.40
	7.0	2.37	0.45
	7.5	2.42	0.38
PSA 3 s	**3.5**	-1.98	0.62
	4.0	-1.29	0.62
	4.5	-0.60	0.62
	5.0	-0.16	0.48
	5.5	0.39	0.46
	6.0	0.88	0.40
	6.5	1.30	0.37
	7.0	1.89	0.41
	7.5	1.99	0.36

Table 15b Median values and standard deviation for reverse fault

GMP	Mw	Median	Standard deviation
PGA	**3.5**	0.63	0.92
	4.0	0.93	0.84
	4.5	1.20	0.79
	5.0	1.22	0.53
	5.5	1.50	0.50
	6.0	1.84	0.50
	6.5	2.00	0.45
	7.0	2.17	0.41
	7.5	2.19	0.35
PSA 0.3 s	**3.5**	0.12	0.61
	4.0	0.60	0.54
	4.5	1.14	0.58
	5.0	1.44	0.48
	5.5	1.75	0.46
	6.0	2.12	0.48
	6.5	2.29	0.43
	7.0	2.48	0.40
	7.5	2.51	0.35
PSA 1.0 s	**3.5**	-0.88	0.57
	4.0	-0.20	0.56
	4.5	0.53	0.59
	5.0	0.75	0.43
	5.5	1.23	0.42
	6.0	1.71	0.44
	6.5	1.95	0.40
	7.0	2.17	0.37
	7.5	2.22	0.33
PSA 3 s	**3.5**	-1.98	0.62
	4.0	-1.29	0.62
	4.5	-0.60	0.62
	5.0	-0.39	0.42
	5.5	0.20	0.39
	6.0	0.90	0.41
	6.5	1.32	0.37
	7.0	1.68	0.34
	7.5	1.79	0.32

Table 15c Median values and standard deviation for strike-slip fault

GMP	Mw	Median	Standard deviation
PGA	**3.5**	0.63	0.92
	4.0	0.93	0.84
	4.5	1.20	0.79
	5.0	1.22	0.58
	5.5	1.44	0.56
	6.0	1.71	0.55
	6.5	1.84	0.52
	7.0	2.11	0.57
	7.5	2.13	0.58
PSA 0.3 s	**3.5**	0.12	0.61
	4.0	0.60	0.54
	4.5	1.14	0.58
	5.0	1.47	0.53
	5.5	1.70	0.52
	6.0	1.99	0.52
	6.5	2.14	0.49
	7.0	2.50	0.58
	7.5	2.44	0.56
PSA 1.0 s	**3.5**	-0.88	0.57
	4.0	-0.20	0.56
	4.5	0.53	0.59
	5.0	0.78	0.49
	5.5	1.19	0.47
	6.0	1.59	0.48
	6.5	1.81	0.45
	7.0	2.13	0.50
	7.5	2.18	0.51
PSA 3 s	**3.5**	-1.98	0.62
	4.0	-1.29	0.62
	4.5	-0.60	0.62
	5.0	-0.37	0.47
	5.5	0.18	0.45
	6.0	0.78	0.44
	6.5	1.19	0.41
	7.0	1.73	0.49
	7.5	1.76	0.47

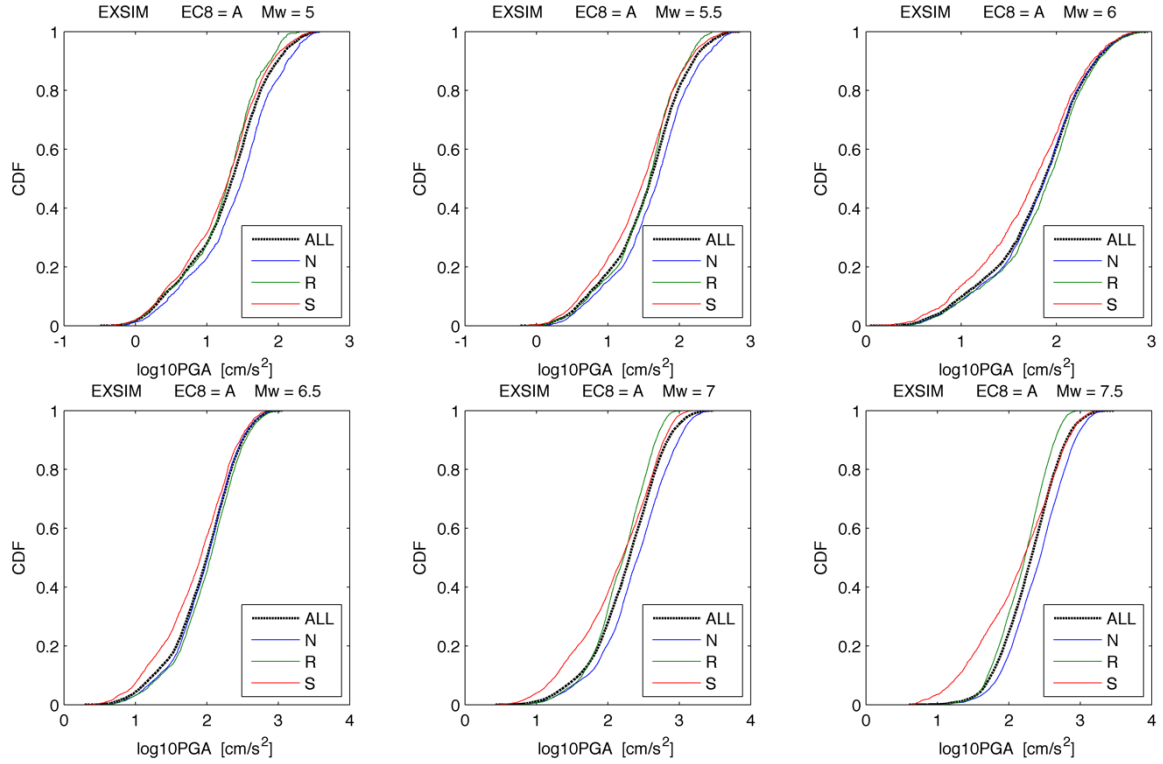

Fig 22 PGA parametric variability of the GS simulations by EXSIM (M_W = 5.0, 5.5, 6.0, 6.5, 7.0, and 7.5). CDFs are computed grouping scenario events that share different style of faulting (N: normal; R: reverse; S: strike-slip); all CDFs are compared to the overall distribution of the PGAs (black curves).

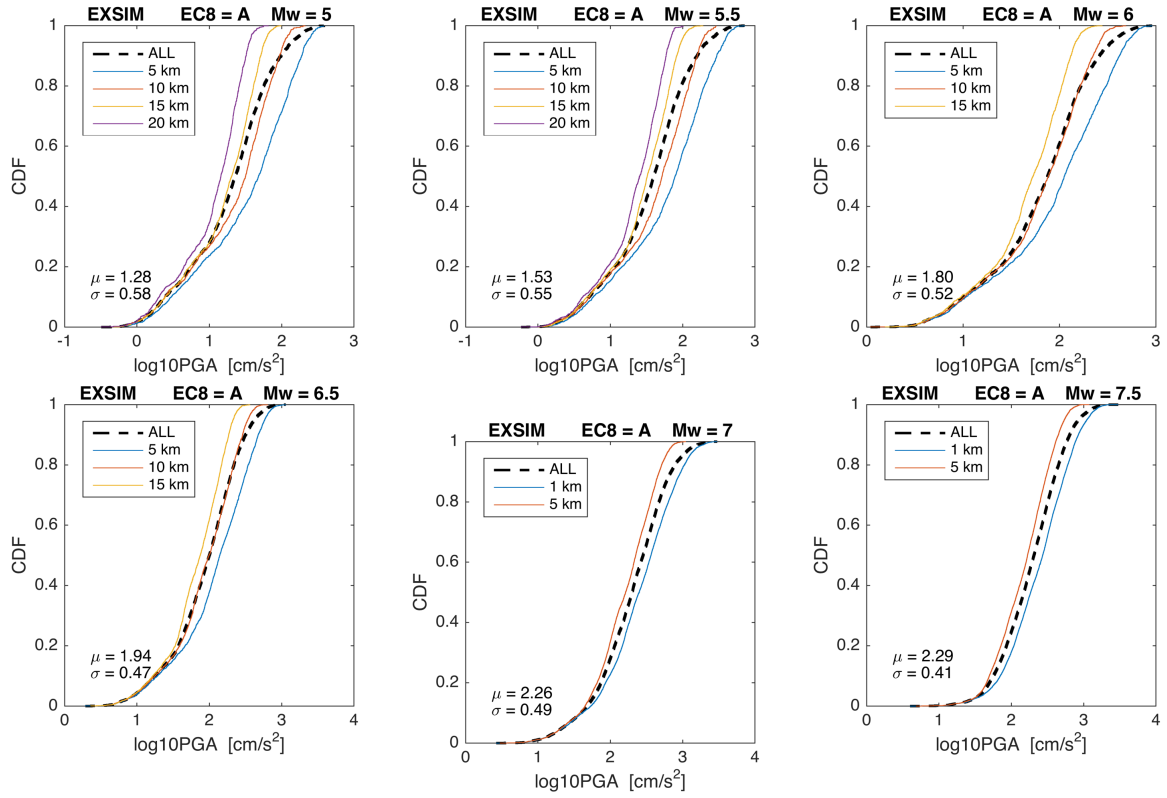

Fig 23 PGA parametric variability of the GS simulations by EXSIM (M_W = 5.0, 5.5, 6.0, 6.5, 7.0, and 7.5). CDFs are computed grouping scenario events that share different top fault depths; all CDFs are compared to the overall distribution of the PGAs (black curves).

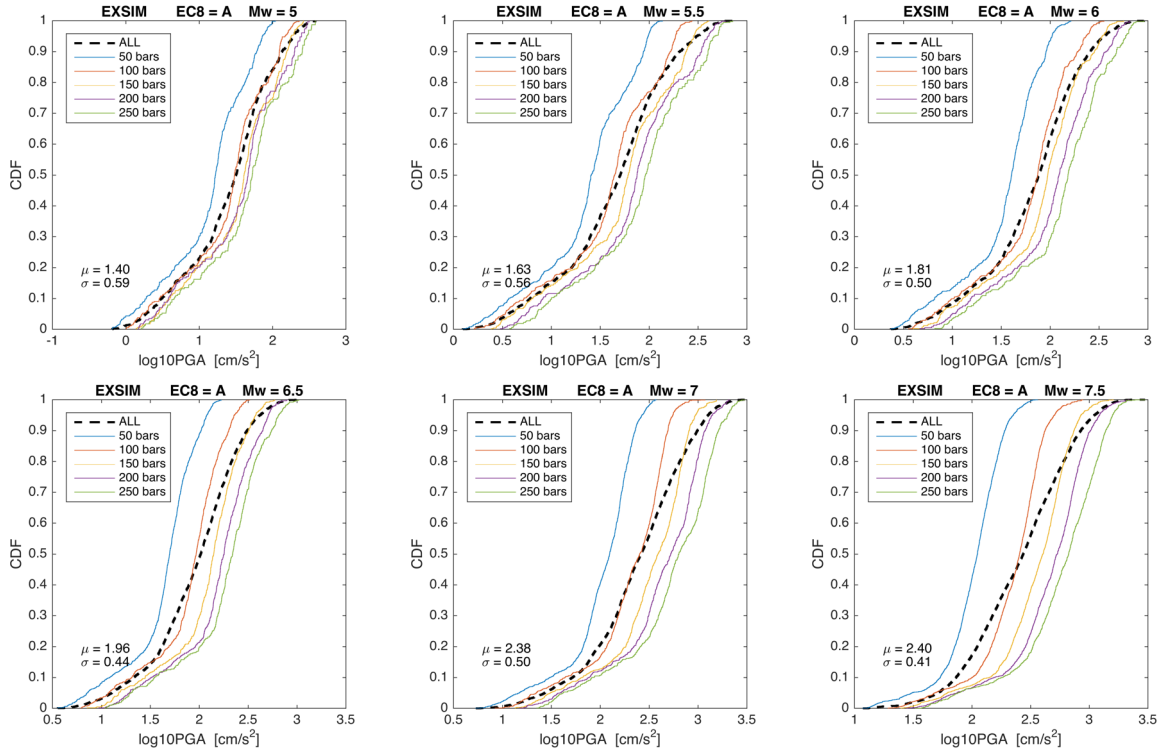

Fig 24 PGA parametric variability of the GS simulations by EXSIM (M_W = 5.0, 5.5, 6.0, 6.5, 7.0, and 7.5). CDFs are computed grouping scenario events that share different stress parameters; all CDFs are compared to the overall distribution of the PGAs (black curves).

References

Atkinson, G.M., Assatourians, K. (2015) Implementation and Validation of EXSIM (A Stochastic Finite-Fault Ground-Motion Simulation Algorithm) on the SCEC Broadband Platform. Seismological Research Letters 86:48–60. doi: 10.1785/0220140097

Atkinson, G.M., Beresnev, I.A. (2002) Ground Motions at Memphis and St. Louis from M 7.5–8.0 Earthquakes in the New Madrid Seismic Zone. Bulletin of the Seismological Society of America 92:1015–1024.

Atkinson, G.M., Boore, D.M. (2006) Earthquake Ground-Motion Prediction Equations for Eastern North America. Bulletin of the Seismological Society of America 96:2181–2205. doi: 10.1785/0120050245

Basili, R., Valensise, G., Vannoli, P., Burrato, P., Fracassi, U., Mariano, S., Tiberti, M.M., Boschi, E. (2008) The Database of Individual Seismogenic Sources (DISS), version 3: Summarizing 20 years of research on Italy's earthquake geology, Tectonophysics, 453, 20-43, doi:10.1016/j.tecto.2007.04.014.

Barberi, G., Cosentino, M.T., Gervasi, A., Guerra, I., Neri, G., Orecchio, B. (2004) Crustal seismic tomography in the Calabrian Arc region, south Italy, Phys. Earth Planet. In. 147, 297–314, doi: 10.1016/j. pepi.2004.04.005.

Bindi, D., F. Pacor, L. Luzi, R. Puglia, M. Massa, G. Ameri, and R. Paolucci (2011) Ground motion prediction equations derived from the Italian strong motion database. Bull Earthquake Eng 9:1899–1920. doi: 10.1007/s10518-011-9313-z

Bindi, D., M. Massa, L. Luzi, G. Ameri, F. Pacor, R. Puglia, and P. Augliera (2014) Pan-European ground-motion prediction equations for the average horizontal component of PGA, PGV and 5%-damped PSA at spectral periods up to 3.0 s using the RESORCE dataset, Bull. Earthq. Eng. 12, 391–430. doi: 10.1007/s10518-013-9525-5

Boore, D.M., Joyner, W.B. (1997) Site amplifications for generic rock sites. Bulletin of the Seismological Society of America, 87, 327-341.

Boore, D.M. (2005) SMSIM—Fortran Programs for Simulating Ground Motions from Earthquakes: Version 2.3—A Revision of OFR 96-80- A, U.S. Geol. Surv. Open-File Report 00-509, revised 15 August 2005, 55 pp. Available from the online publications link on https://profile .usgs.gov/professional/mypage.php?name=boore.

Boore, D.M. (2003) Simulation of Ground Motion Using the Stochastic Method. Pure Appl Geophys 160:635–676. doi: 10.1007/PL00012553

Boore, D.M. (2009) Comparing Stochastic Point-Source and Finite-Source Ground-Motion Simulations: SMSIM and EXSIM. Bulletin of the Seismological Society of America 99:3202–3216. doi: 10.1785/0120090056

Boore, D.M., Stewart, J.P., Seyhan, E., Atkinson, G.M. (2014) NGA-West2 Equations for Predicting PGA, PGV, and 5% Damped PSA for Shallow Crustal Earthquakes. Earthquake Spectra 30:1057–1085. doi: 10.1193/070113EQS184M

Bordoni, P., Valensise, G. (1998) Deformation of the 125 ka marine terrace in Italy: tectonic implications, Geol. Soc. Spec. Publ., 146, 71-110, doi:10.1144/gsl.sp.1999.146.01.05.

Bottari, A., Capuano, P., De Natale, G., Gasparini, P., Neri, G., Pingue, F., Scarpa, R. (1989) Source parameters of earthquakes in the Strait of Messina, Italy, during this century. Tectonophysics, 166, 221-234.

Caporali, A., Barba, S., Carafa, M., Devoti, R., Pietrantonio, G., Riguzzi, F. (2011) Static stress drop as determined from geodetic strain rates and statistical seismicity. *Journal of Geophysical Research: Solid Earth*, *116*(B2).

Cauzzi, C., Faccioli, E., Vanini, M., Bianchini, A. (2014) Updated predictive equations for broadband (0.01–10 s) horizontal response spectra and peak ground motions, based on a global dataset of digital acceleration records. Bull Earthquake Eng 13:1587–1612. doi: 10.1007/s10518-014-9685-y

Cernobori, L., Hirn, A., McBride, J. H., Nicolich, R., Petronio, L., Romanelli M. (1996) Crustal image of the Ionian basin and its Calabrian margins, Tectonophysics, 264, 175-189, doi:http://dx.doi.org/10.1016/S0040-1951(96)00125-4.

Chiarabba, C., Jovane, L., Di Stefano R. (2005) A new view of Italian seismicity using 20 years of instrumental recordings, Tectonophysics, 395, 251-268, doi:10.1016/j.tecto.2004.09.013.

Chiarabba, C., De Gori, P., Mele, F. M. (2015) Recent seismicity of Italy: Active tectonics of the central Mediterranean region and seismicity rate changes after the Mw 6.3 L'Aquila earthquake, Tectonophysics, 638, 82-93, doi:10.1016/j.tecto.2014.10.016.

Cifelli, F., Mattei, M., Della Seta M. (2008) Calabrian Arc oroclinal bending: The role of subduction, Tectonics, 27, n/a-n/a, doi:10.1029/2008tc002272.

D'Amico, S. (2010) Development of ground motion attenuation relationships for southern Italy based on attenuation models and stochastic simulations. PhD Thesis.

D'Amico, S., Orecchio, B., Presti, D., Gervasi, A., Zhu, L., Guerra, I., Neri, G., Herrmann, R. (2011) Testing the stability of moment tensor solutions for small earthquakes in the Calabro-Peloritan Arc region (southern Italy), Boll. Geof. Teor. Appl. 52, 283–298, doi: 10.4430/ bgta0009.

D'Amico M., Tiberti, M. M., Russo, E., Pacor, F., Basili, R. (2017) Ground-motion variability for single site and single source through deterministic stochastic method simulations: implications for PSHA. Bull. Seism. Soc. Am., 107 (2), 966-983, doi: 10.1785/0120150377.

Devoti, R., Riguzzi, F., Cuffaro, M., Doglioni, C. (2008) New GPS constraints on the kinematics of the Apennines subduction, Earth Planet. Sc. Lett., 273, 163-174, doi:http://dx.doi.org/10.1016/j.epsl.2008.06.031.

Dreger, D.S., Jordan, T.H. (2015) Introduction to the Focus Section on Validation of the SCEC Broadband Platform V14.3 Simulation Methods. Seismological Research Letters 86:15–16. doi: 10.1785/0220140233

Faccenna, C. (2005) Constraints on mantle circulation around the deforming Calabrian slab, Geophys. Res. Lett., 32, doi:10.1029/2004gl021874.

Faccenna, C., Funiciello, F., Giardini, D., Lucente, F. P. (2001) Episodic back-arc extension during restricted mantle convection in the Central Mediterranean, Earth Planet. Sc. Lett., 187, 105-116.

Ferranti, L., Antonioli, F., Mauz, B., Amorosi, A., Dai Pra, G., Mastronuzzi, G., Monaco, C., Orrù, P., Pappalardo, M., Radtke, U., Renda, P., Romano, P., Sansò, P., Verrubbi, V. (2006) Markers of the last interglacial sea-level high stand along the coast of Italy: Tectonic implications, Quatern. Int., 145-146, 30-54, doi:10.1016/j.quaint.2005.07.009.

Gasparini, C., Iannaccone, G., Scarpa. R. (1985) Fault-plane solutions and seismicity of the Italian peninsula. Tectonophysics, 117: 59-78.

Goulet, C.A., Abrahamson, N.A., Somerville, P.G., Wooddell, K.E. (2015) The SCEC Broadband Platform Validation Exercise: Methodology for Code Validation in the Context of Seismic-Hazard Analyses. Seismological Research Letters 86:17–26. doi: 10.1785/0220140104

Faenza, L., Michelini, A. (2011) Regression analysis of MCS intensity and ground motion spectral accelerations (SAs) in Italy. Geophysical Journal International 186:1415–1430. doi: 10.1111/j.1365-246X.2011.05125.x

Frepoli, A., Amato, A., (2000) Fault-plane solutions of crustal earthquakes in southern Italy (1988-
471 1995): seismotectonic implications. Ann. Geofis. 43, 437-467.

Giampiccolo, E., Tusa, G., Langer, H., Gresta, S., (2002) Attenuation in southeastern Sicily (Italy) by applying different coda methods, J. Seismol., 6, 487–501.

Giampiccolo, E., Tuvè, T., Gresta, S., Patanè, D., (2006) S-waves attenuation and separation of scattering and intrinsic absorption of seismic energy in southeastern Sicily (Italy). Geophys. J. Int. 165, 211–222.

Godano, A., Bottari, A., Cocina, O., Del Pezzo, E., Marino, A., (1992) Depth dependence of seismic attenuation in the Messina Strait area. Tectonophysics 206, 137–146.

Goes, S., Giardini, D., Jenny, S., Hollenstein, C., Kahle, H. G., Geiger, A. (2004) A recent tectonic reorganization in the south-central Mediterranean, Earth Planet. Sc. Lett., 226, 335-345, doi:10.1016/j.epsl.2004.07.038.

Hanks, T. C., Kanamori, H. A. (1979) moment magnitude scale. J. Geophys. Res 84: 2348-2349.

Locati M., Camassi R., Rovida A., Ercolani E., Bernardini F., Castelli V., Caracciolo C.H., Tertulliani A., Rossi A., Azzaro R., D'Amico S., Conte S., Rocchetti E. (2016) DBMI15, the 2015 version of the Italian Macroseismic Database. Istituto Nazionale di Geofisica e Vulcanologia. doi:http://doi.org/10.6092/INGV.IT-DBMI15

Kanamori, Hiroo, and Don L. Anderson. Theoretical basis of some empirical relations in seismology. Bulletin of the Seismological Society of America 65.5 (1975): 1073-1095.

Maesano, F.E., Tiberti, M.M., Basili, R. (2017) The Calabrian Arc: three-dimensional modelling of the subduction interface. Scientific Reports, 7, 8887, doi:10.1038/s41598-017-09074-8.

Margottini, C., Molin, D., Serva, L. (1992) Intensity versus ground motion: a new approach using Italian data. Eng Geol 33(1):45–58. doi:10.1016/0013-7952(92)90034-V

Merlini, S., Cantarella, G., Doglioni, C. (2000) On the seismic profile Crop M5 in the Ionian Sea, B. Soc. Geol. Ital., 119, 227-236.

Minelli, L., Faccenna, C. (2010) Evolution of the Calabrian accretionary wedge (central Mediterranean), Tectonics, 29, doi:10.1029/2009tc002562.

Motazedian, D., Atkinson, G.M. (2005) Stochastic finite-fault modeling based on a dynamic corner frequency. Bulletin of the Seismological Society of America 95:995–1010. doi: 10.1785/0120030207

Neri, G., Orecchio, B., Totaro, C., Falcone, G., Presti, D. (2009) Subduction Beneath Southern Italy Close the Ending: Results from Seismic Tomography, Seismological Research Letters, 80(1), 63-70, doi:10.1785/gssrl.80.1.63.

Neri, G., Wyss, M., (1993) Preliminary results from stress tensor inversion of earthquake fault plane solutions in the Southern Tyrrhenian region, Boll. Geof. Teor. Appl., XXXV, 139, 349-362.

Neri, G., Caccamo, D., Cocina, O., Montalto, A., (1996) Geodynamic implications of earthquake data in the Southern Tyrrhenian Sea, Tectonophysics, 258, 233-249.

Nocquet, J.M. (2012) Present-day kinematics of the Mediterranean: A comprehensive overview of GPS results, Tectonophysics, 579, 220-242, doi:10.1016/j.tecto.2012.03.037.

Orecchio, B., Presti, D., Totaro, C., Guerra, I., Neri, G. (2011) Imaging the velocity structure of the Calabrian Arc region (southern Italy) through the integration of different seismological data, Boll. Geof. Teor. Appl. 52, 625–638, doi: 10.4430/bgta0023.

Pacor, F., Cultrera, G., Mendez, A., Cocco, M. (2005) Finite fault mod- eling of strong ground motion using a hybrid deterministic—stochastic method, Bull. Seismol. Soc. Am. 95, 225–240.

Piana Agostinetti, N., Steckler, M. S., Lucente, F. P. (2009) Imaging the subducted slab under the Calabrian Arc, Italy, from receiver function analysis, Lithosphere-US, 1, 131-138, doi:10.1130/l49.1.

Piromallo, C., Morelli, A. (2003) Pwave tomography of the mantle under the Alpine-Mediterranean area, J. Geophys. Res., 108, doi:10.1029/2002jb001757.

Polonia, A., Torelli, L., Mussoni, P., Gasperini, L., Artoni, A., Klaeschen, D. (2011) The Calabrian Arc subduction complex in the Ionian Sea: Regional architecture, active deformation, and seismic hazard, Tectonics, 30, doi:10.1029/2010tc002821.

Pondrelli, S., Salimbeni, S., Ekström, G., Morelli, A., Gasperini, P., Vannucci, G. (2006) The Italian CMT dataset from 1977 to the present, Phys. Earth Planet. In., 159, 286-303, doi:http://dx.doi.org/10.1016/j.pepi.2006.07.008.

Rovida A., Locati M., Camassi R., Lolli B., Gasperini P. (eds), 2016. CPTI15, the 2015 version of the Parametric Catalogue of Italian Earthquakes. Istituto Nazionale di Geofisica e Vulcanologia. doi:http://doi.org/10.6092/INGV.IT-CPTI15

Scognamiglio, L., Malagnini, L., Akinci A. (2005) Ground-Motion Scaling in Eastern Sicily, Italy, Bulletin of the Seismological Society of America, 95, 568-578; DOI: 10.1785/0120030124.

Tiberti, M.M., Vannoli, P., Fracassi, U., Burrato, P., Kastelic, V., Valensise, G. (2016) Understanding seismogenic processes in the Southern Calabrian Arc: a geodynamic perspective, Italian Journal of Geosciences, 10.3301/IJG.2016.12

Tuvè, T., Bianco, F., Ibáñez, J., Patané, D., Del Pezzo, E., Bottari, A. (2006) Attenuation study in the Straits of Messina area (southern Italy). Tectonophysics 421:173–185. doi: 10.1016/j.tecto.2006.04.005

Wells D.L., Coppersmith, K.J. (1994) New Empirical Relationships among Magnitude, Rupture Length, Rupture Width, Rupture Area, and Surface Displacement. Bulletin of the Seismological Society of America, 84, 974-1002.

Wortel, M., Spakman, W. (2000) Subduction and slab detachment in the Mediterranean-Carpathian region, Science, 290, 1910-1917.

Appendix

Modeling LogPGA from Macroseismic Intensity

A new empirical relationship between PGAen and macroseismic intensity is developed in the present work by comparing the recorded largest of the horizontal components (peak ground motion) to observed macroseismic intensities from 78 strong-motion stations selected by D3.1DPC-INGV-S2-Project, (https://goo.gl/hLYZXY).
The input data set correspond to 118 pairs of Log(PGAen)-Macroseismic intensity from 53 Italian earthquakes in the time-window 1976-2009, with Mw ranging from [3.90 - 6.90] and span a macroseimic intensity [3/4 – 8/9]. The input dataset is given by Tab. 1, more details are given by Gomez Capera et al. (2015).
The methodology used (Bilal and Askan, 2014; Tselentis and Danciu, 2008) is given by a predictive non-linear relationship between logarithm of PGAen(cm/s^2), the macroseismic intensity (I), the moment magnitude (Mw) and the logarithm of distance (x) between the PGA-station and the epicenter of the event (Tab.1), the obtained empirical relationship is:

$$\text{Log10(PGAen)} = (0.616\pm0.26) + (0.154\pm0.05)\text{I} + (0.221\pm0.05)\text{Mw} - (0.510\pm0.07)\text{Log10(x)} \quad [1]$$

The variance is 0.17. The input dataset and the obtained empirical relationship is plotted in fig. 1. The fitting model was made using Wolfram Mathematica 9.

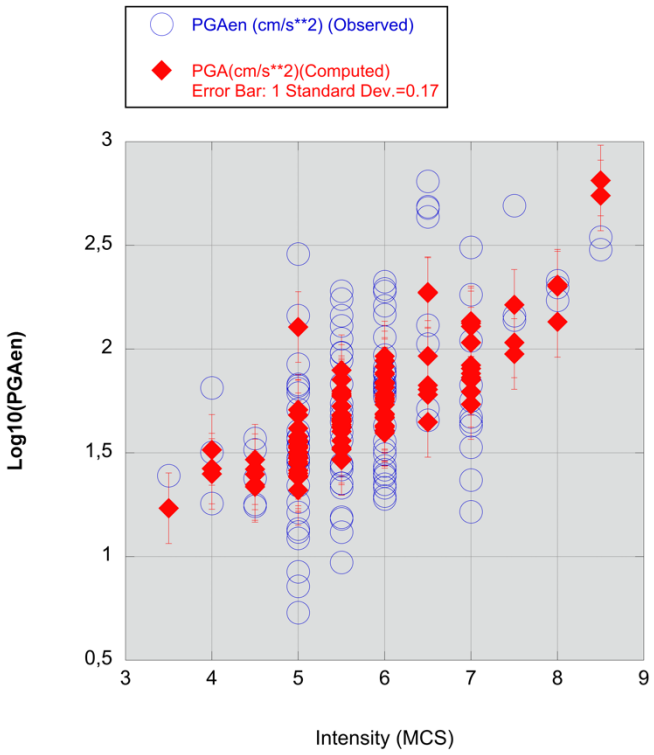

Fig. 1. Input data set (blue circle) and modeled data using equation [1]

Tab1. Table coupling macroseismic intensity data and PGAen Earthquake parameters (Date and time, moment magnitude Mw) are by Italian earthquake catalogue (CPTI11, Rovida et al., 2011). Macroseismic Intensity (I) by Italian Macroseismic Database (DBM11, Locati et al., 2011). The PGAen data are (code of *Stz., distance between epicenter event and *Stz.) by ITACA (Luzi et al., 2018).

N	Ye	Mo	Da	h	m	s	Mw	I	*Stz.	Dist.	Log (Dist.)	Log (PGA_{en})
1	1976	5	6	20	0	12	6,46	7	BRC	54,9	1,740	1,527
2	1976	5	6	20	0	12	6,46	6	CNG	86,6	1,938	1,837
3	1977	7	24	9	55	28	4,43	5,5	ARI	11,0	1,041	1,182
4	1978	4	15	23	33	47	6,06	7,5	NAS	33,0	1,519	2,162
5	1978	4	15	23	33	47	6,06	5	GRR	60,5	1,782	1,453
6	1979	9	19	21	35	37	5,86	8	CSC	9,3	0,968	2,297
7	1979	9	19	21	35	37	5,86	5,5	MNF	31,2	1,494	0,972
8	1979	9	19	21	35	37	5,86	5	BVG	38,0	1,580	1,532
9	1979	9	19	21	35	37	5,86	6	NCR	40,4	1,606	1,887
10	1980	11	23	18	34	52	6,89	8	CLT	18,9	1,276	2,235
11	1980	11	23	18	34	52	6,89	7	BGI	21,9	1,340	2,263
12	1980	11	23	18	34	52	6,89	7	ALT	23,4	1,369	1,751
13	1980	11	23	18	34	52	6,89	7	STR	33,3	1,522	2,491
14	1980	11	23	18	34	52	6,89	8	BRN	42,6	1,629	2,329
15	1980	11	23	18	34	52	6,89	7,5	MRT	47,1	1,673	2,140
16	1980	11	23	18	34	52	6,89	7	BVN	54,4	1,736	1,674
17	1980	11	23	18	34	52	6,89	7	BNV	58,7	1,769	1,650
18	1980	11	23	18	34	52	6,89	7	SGR	65,4	1,816	1,216
19	1980	11	23	18	34	52	6,89	6,5	TRR	73,2	1,865	1,657
20	1980	11	23	18	34	52	6,89	6	TDG	78,4	1,894	1,769
21	1980	11	23	18	34	52	6,89	6	SSV	102,5	2,011	1,332
22	1981	6	7	13	0	57	4,96	6	MZR	9,7	0,987	2,278
23	1982	3	21	9	44	2	5,36	7	LRS	41,6	1,619	1,369
24	1982	10	17	4	54	35	4,61	5,5	NCR	10,7	1,029	1,981
25	1982	10	17	6	45	37	4,61	4	NCR	8,1	0,908	1,813
26	1983	11	9	16	29	52	5,06	6	FRN	21,0	1,322	1,519
27	1984	4	29	5	2	60	5,65	6	GBB	16,5	1,217	1,818
28	1984	4	29	5	2	60	5,65	4	UMB	26,0	1,415	1,502
29	1984	4	29	5	2	60	5,65	5,5	PTL	26,1	1,417	2,241
30	1984	4	29	5	2	60	5,65	5	CGL	36,5	1,562	0,856
31	1984	4	29	5	2	60	5,65	5	PGL	54,3	1,735	1,710
32	1984	5	7	17	49	43	5,89	6	PNT	26,8	1,428	1,821
33	1984	5	7	17	49	43	5,89	7	STG	34,3	1,535	1,827
34	1984	5	7	17	49	43	5,89	7	RCC	46,8	1,670	1,631
35	1984	5	7	17	49	43	5,89	6	BSS	54,6	1,737	1,349
36	1984	5	7	17	49	43	5,89	6,5	SCF	63,8	1,805	2,116
37	1984	5	7	17	49	43	5,89	7	ATN	10,1	1,004	2,040
38	1984	5	7	17	49	43	5,89	5	BRS	72,9	1,863	1,087
39	1984	5	11	10	41	50	5,50	6	ATN	19,2	1,283	1,396
40	1984	5	11	10	41	50	5,50	6	STG	37,1	1,569	1,419
41	1984	5	11	10	41	50	5,50	5,5	SCF	54,6	1,737	1,599
42	1985	5	20	10	0	30	4,58	4,5	BRS	19,1	1,281	1,515
43	1985	11	24	6	54	4	4,32	4,5	PNN	19,9	1,299	1,569
44	1987	5	2	20	43	53	4,74	6	NVL	6,9	0,839	1,876
45	1987	7	5	15	12	37	4,47	5	PGL	24,4	1,387	1,824
46	1988	2	1	14	21	38	4,65	5	TLM2	7,0	0,845	1,133

47	1988	3	15	12	3	18	4,66	5,5	NVL	4,2	0,623	1,438
48	1989	3	11	21	5	59	4,52	4	SSV	12,8	1,107	1,256
49	1989	3	11	21	5	59	4,52	5	SNN	18,0	1,255	1,607
50	1989	9	13	21	54	1	4,88	5	MLC	26,7	1,427	1,567
51	1990	5	5	7	21	22	5,80	6	TRR	25,2	1,401	1,555
52	1990	5	5	7	21	22	5,80	5,5	BRN	26,1	1,417	1,983
53	1990	5	5	7	21	22	5,80	5,5	GRM	36,7	1,565	1,447
54	1990	5	5	7	21	22	5,80	6	CLT	45,7	1,660	1,494
55	1990	12	13	0	24	28	5,64	6,5	SRT	26,2	1,418	2,024
56	1991	1	14	7	38	36	4,47	4,5	STS	12,8	1,107	1,377
57	1991	5	26	12	26	1	5,11	5,5	TRR	31,6	1,500	1,333
58	1991	5	26	12	26	1	5,11	5	GRM	42,3	1,626	1,474
59	1992	4	6	13	8	38,88	4,76	5	NCS	16,5	1,217	1,342
60	1993	6	4	21	36	51	4,50	5,5	NCR	5,9	0,771	2,162
61	1993	6	5	19	16	17	4,74	5,5	NCR	15,2	1,182	2,279
62	1995	9	30	10	14	34	5,18	5,5	SNN	28,6	1,456	2,051
63	1996	4	3	13	4	36	4,93	5	STR	49,1	1,691	1,213
64	1996	10	15	9	56	2	5,41	6	NVL	13,4	1,127	2,290
65	1997	9	3	22	7	30	4,56	5	NCR	12,7	1,104	2,459
66	1997	9	7	23	28	6	4,38	5	NCR	11,6	1,064	1,809
67	1997	9	26	0	33	13	5,70	6,5	NCR	13,2	1,121	2,687
68	1997	9	26	0	33	13	5,70	6	MNF	24,2	1,384	1,388
69	1997	9	26	0	33	13	5,70	6,5	BVG	25,0	1,398	1,712
70	1997	9	26	0	33	13	5,70	5,5	MTL	26,9	1,430	1,678
71	1997	9	26	0	33	13	5,70	6	CSC	35,2	1,547	1,437
72	1997	9	26	9	40	27	6,01	7,5	NCR	10,9	1,037	2,692
73	1997	9	26	9	40	27	6,01	6	BVG	23,2	1,365	1,890
74	1997	9	26	9	40	27	6,01	6	MTL	27,0	1,431	2,057
75	1997	9	26	9	40	27	6,01	5,5	CSC	36,8	1,566	1,332
76	1997	9	26	9	40	27	6,01	6	GBB	42,1	1,624	1,912
77	1997	9	26	9	40	27	6,01	6	PTL	55,4	1,744	1,835
78	1997	9	26	9	40	27	6,01	6	CGL	59,1	1,772	1,292
79	1997	9	26	9	40	27	6,01	5,5	SNG	78,5	1,895	1,649
80	1997	9	26	9	40	27	6,01	5,5	PGL	79,5	1,900	1,832
81	1997	10	3	8	55	20,64	5,25	5,5	BVG	22,6	1,354	1,354
82	1997	10	3	8	55	20,64	5,25	5	MNF	27,5	1,439	1,119
83	1997	10	3	8	55	20,64	5,25	4,5	GBB	40,9	1,612	1,252
84	1997	10	6	23	24	53	5,46	5,5	BVG	21,9	1,340	1,707
85	1997	10	6	23	24	53	5,46	6	MNF	27,6	1,441	1,278
86	1997	10	6	23	24	53	5,46	5	CSC	36,3	1,560	1,263
87	1997	10	6	23	24	53	5,46	5,5	GBB	42,4	1,627	1,560
88	1997	10	14	15	23	11	5,65	6	CSC	24,3	1,386	1,793
89	1997	10	14	15	23	11	5,65	5,5	MNF	25,3	1,403	1,191
90	1997	10	14	15	23	11	5,65	6	BVG	26,0	1,415	1,631
91	1997	11	9	19	7	33	4,90	5,5	CSC	14,3	1,155	1,118
92	1998	3	26	16	26	16,6	5,29	5	MTL	19,9	1,299	1,574
93	1998	3	26	16	26	16,6	5,29	4,5	BVG	28,7	1,458	1,243
94	1998	4	5	15	52	20,7	4,81	5	NCR	8,8	0,944	2,162
95	1998	9	9	11	28	1,2	5,64	6	LRS	9,9	0,996	2,209
96	1998	11	8	22	33	42,6	4,31	5	LRS	0,9	-0,046	0,927
97	1999	1	16	0	19	42,9	4,16	5,5	LRS	5,0	0,699	1,353
98	1999	2	14	11	45	54,1	4,69	6	NAS	23,8	1,377	1,810
99	1999	3	14	22	1	1	3,88	5	LRS	11,4	1,057	0,730
100	2000	8	21	17	14	28	4,86	5,5	NZZ	6,0	0,778	2,112

101	2000	12	16	7	31	8	4,25	5,5	NRN	5,5	0,740	1,738
102	2002	11	1	15	9	2	5,72	3,5	SSV	45,9	1,662	1,391
103	2003	1	26	19	57	3,21	4,70	6	STS	6,5	0,813	1,971
104	2003	1	26	20	15	4,2	4,56	6	STS	5,1	0,708	2,325
105	2003	4	11	9	26	57,9	4,85	5	TRT	16,4	1,215	1,927
106	2009	4	6	1	32	40	6,30	8,5	AQK	1,8	0,255	2,540
107	2009	4	6	1	32	40	6,30	8,5	AQU	2,5	0,398	2,480
108	2009	4	6	1	32	40	6,30	6,5	AQG	5,1	0,708	2,681
109	2009	4	6	1	32	40	6,30	**6,5**	AQV	5,1	0,708	2,809
110	2009	4	6	1	32	40	6,30	6,5	AQA	5,2	0,716	2,637
111	2009	4	6	1	32	40	6,30	6	GSA	14,6	1,164	2,166
112	2009	4	6	1	32	40	6,30	5,5	FMG	23,1	1,364	1,420
113	2009	4	6	1	32	40	6,30	5	MTR	23,3	1,367	1,788
114	2009	4	6	1	32	40	6,30	5	ANT	26,3	1,420	1,414
115	2009	4	6	1	32	40	6,30	5,5	CLN	30,6	1,486	1,947
116	2009	4	6	1	32	40	6,30	5	AVZ	34,9	1,543	1,831
117	2009	4	6	1	32	40	6,30	5	SUL	53,6	1,729	1,526
118	2009	4	6	1	32	40	6,30	5	CHT	63,3	1,801	1,469

References

Bilal M., Askan A. (2014) Relationships between felt intensity and recorded ground-motion parameters for Turkey. *Bull Seismol Soc Am* 104(1):484–486. doi:10.1785/0120130093

Gómez Capera, A.A., Locati, M., Fiorini, E., Bazurro P., Luzi, L., Massa, M., Puglia, R., Santulin, M. (2015) D3.1 Macroseismic and ground motion: site specific conversion rules. DPC-INGV-S2 Project "Constraining observations into Sesismic Hazard", deliverable D3.1, 23.06.2015, Milano, 66pp.

Locati, M., Camassi, R., Stucchi, M. (eds.) (2011) DBMI11, the 2011 version of the Italian Macroseismic Database. Istituto Nazionale di Geofisica e Vulcanologia, Milano, Bologna. doi:10.6092/INGV.IT- DBMI11

Luzi, L., Hailemikael, S., Bindi, D., Pacor, F., Mele, F., Sabetta, F. (2008) Itaca (Italian Accelerometric Archive): a web portal for the dissemination of Italian strong-motion data, *Seism. Res. Lett*., 79(5), 716–722.

Rovida, A., Camassi, R., Gasperini, P., Stucchi, M. (eds.) (2011) CPTI11, the 2011 version of the Parametric Catalogue of Italian Earthquakes. Istituto Nazionale di Geofisica e Vulcanologia, Milano, Bologna. doi:10.6092/INGV.IT-CPTI11.

Tselentis, G., Danciu, L. (2008) Empirical relationships between modified Mercalli intensity and engineering ground-motion parameters in Greece. *Bull Seismol Soc Am* 98(4):1863–1875. doi:10.1785/ 0120070172

Disclaimer

Any result included in the document is based on the available scientific knowledge and is devoted to qualified users. Every risk due to the improper use of data or the use of inaccurate information is assumed by the user.

Creative Commons

Citation

This Deliverable must be cited as follow: "D'Amico M, Tiberti MM, Russo E, Gomez-Capera A (2018). Ground motion simulation. Istituto Nazionale di Geofisica e Vulcanologia, HYPSTHER project, http://hypsther.mi.ingv.it/ - doi: 10.5281/zenodo.1162203".